Photocatalytic Degradation of Industrial Dye Using Catalysts Synthesized Via Nanogrinding

by

Xue Cai

B. Sc., Northwest A&F University of China, 2014

A Project Report Submitted in Partial Fulfillment

of the Requirements for the Degree of

MASTER OF ENGINEERING

in the Department of Electrical & Computer Engineering

Supervisory Committee

Photocatalytic Degradation of Industrial Dye Using Catalysts Synthesized Via Nanogrinding

by

Xue Cai

B. Sc., Northwest A&F University of China, 2014

Dr. Christo Papadopoulos (Department of Electrical & Computer Engineering)

Supervisor

Dr. Mihai Sima (Department of Electrical & Computer Engineering)

Departmental Member

Abstract

In recent years, environmental pollution is the most important problem to be solved. As an effective method to control environmental pollution, semiconductor photocatalyst has been widely studied and applied in the field of photocatalysis. Photocatalytic degradation technology is a new pollutant treatment method, which has the advantages of simple operation, low energy consumption, mild reaction conditions and no secondary pollution. In this project, the photocatalyst was prepared by planetary ball milling method (PBM) and used for degradation of organic dyes.

Planetary ball milling method is used to synthesis different kinds of semiconductor nano-photocatalysts. It is a top down approach to mechanically breaking a solid into smaller particles. Chapter 3 presented the details of the preparation including raw materials, devices and the grinding parameters for different grinding trials. Then the process of the grinding was introduced, including measurement, processing and extraction. After the suspension with ZnO nanoparticles was obtained, the nanoparticle powders were prepared by "washing" method and their catalytic properties were tested by degradation experiment.

Several dye degradation experiments were designed to test the catalytic performance of ZnO nanoparticles with different particle sizes prepared by planetary ball mill. Control experiment was conducted to prove that dark reaction can maintain the adsorption equilibrium of dye molecules on the surface of ZnO. The effects of particle size, surface area, bulk defect and surface defect on photocatalytic performance of zinc oxide were discussed.

Table of Content

List of Tables

List of Figures

Acknowledgements

I would like to thank my supervisor Dr. Christo Papadopoulos for his great patience and valuable ideas. I would never finish this project without his guidance. Also, I would like to thank Dr. Mihai Sima for being the member of my supervisory committee and the effort he spent.

Thanks to my parents, I am eternally grateful to them for their unconditional love and support. I am especially thankful to my beloved husband, Dr. Dapeng Liu, who takes care of me beyond my dreams and expectations.

Chapter 1 Introduction

Environmental pollution is one of the most important problems facing humans in this century, among which water pollution has seriously threatened our life safety. At present, the increase in dyeing industry displacement is one of the reasons for the aggravation of water pollution.

Dyeing wastewater is one of the most important pollutants in the world. Some dyes never degrade in water. Other dyes can degrade but produce harmful substances when they decompose.[1] To solve the impact of wastewater on ecological environment, production and living as well as economic benefits is a problem that people pay close attention to. A large number of researchers have invested a lot of manpower and material resources to try and practice.

Generally speaking, the traditional cleaning method is divided into biological method, physical method and chemical method. These methods have been widely used in textile industry, but there are still some deep secondary problems. The advantages of biological treatment are low cost and simple operation, but due to the strong resistance to aerobic biodegradation, the effect is usually poor [2]. Physical treatment is usually effective in removing dyes, but the follow-up of the treatment is complicated [3]. Chemical treatment also has disadvantages, such as producing toxic by-products, requiring large doses of chemicals, incomplete degradation, etc [4-5]. Due to the limitations of existing wastewater treatment systems, it is very important to develop a significantly improved wastewater treatment method, among which semiconductor photocatalytic degradation technology is most promising.

The most successful decolorization methods usually involve oxidative degradation of dyes, known as advanced oxidation methods (AOPs). The semiconductor is prepared

into photocatalytic materials, and organic pollutants are converted into green pollution-free substances such as CO2, H2O, sulfate and nitrate. Since 1972, Fujishima [6] found that TiO2 electrodes can catalyze the decomposition of water and produce H_2 under light conditions, people began to have a strong interest in whether semiconductor photocatalytic technology can be applied to the treatment of water pollution. In 1976, Carey et al. [7] found that nano TiO2 could dechlorinate refractory organic polychlorinated biphenyls (PCBS), and the research on the degradation of organic pollutants by semiconductor materials began to increase worldwide. At present, semiconductor particles are widely used as photocatalytic materials. Photocatalytic photosensitive material, as an environmental protection material, has shown characteristics and advantages that are not found in common materials.

Currently, semiconductor photocatalytic materials are widely used, including TiO2, ZnO, ZrO2, SnO2, WO3 and other materials [8]. Faced with such a wide variety of semiconductor photocatalytic materials, many researchers have made a lot of attempts and improvements. Among all those, zinc oxide has proven to be a promising photocatalyst, because it is a low-cost material that can rapidly catalyze the degradation of dyes under simple operating conditions, and can completely decompose a large number of organic pollutants [9]. ZnO is the main semiconductor photocatalyst used in this project.

1.1 Textile dye

In order to better understand the degradation and decolorization of dyes in textile wastewater, it is better to understand the chemical structure of common dyes and the causes of color generation. This section introduces some basic chemical principles related to colored compounds and outlines how the chemical structure of molecules affects their color properties. The latter part describes dye classification and advanced oxidation process (AOP) for wastewater treatment.

1.1.1 Color and the chemical structure

Many efforts have been made to understand the relationship between color and the chemical structure of dye molecules. In 1876, Witt proposed his theory of color, in which dye molecules must contain both a chromophore and an auxochrome to an aryl ring [10]. In 1907, Hewitt proposed that conjugated systems were essential for the generation of color [11]. Dilthey (1928) combined these concepts and concluded that pheochromocyte and pheochromocyte were electric-absorbing group and electric-supplying group respectively, which are interconnected through the conjugate system [12].

Chromophore: Some groups of the molecular structure absorb light at one wavelength and not the other, thus giving the impression that the substance "gives off color". For this structure, the unsaturated conjugate chain is connected to the group containing electron donor group, as well as the group with different electrical properties [13-14]. After absorbing the quantum energy of light at certain wavelength, the polarization of the compound molecule produces a dipole moment, which causes valence electrons to jump between different energy levels and emit energy in the form of light.

Auxochromes: The basic characteristic of auxochromes is that they have at least one pair of unshared electrons in the group that increase the conjugated system of the molecule by resonance [15]. For example, hydroxyl, amine, or halogen groups do not absorb radiation, but can move the absorption peaks of chromophores in molecules to longer wavelengths and increase their intensity.

1.1.2 Classification of dyes

Classification of Dyes is usually based on Color Index (CI), an international collection of dyes and pigments compiled by the British society of dyeing (SDC) and the American society of textile chemists and dyeing (AATCC). It collects commodities

produced by dye factories around the world and is considered the leading standard index.[16]

According to the color index, there are 19 categories of dyes and 25 structural categories.[17] The main categories of dyes based on method of application (generic name) and chemical constitutions are shown in figure 1.1.

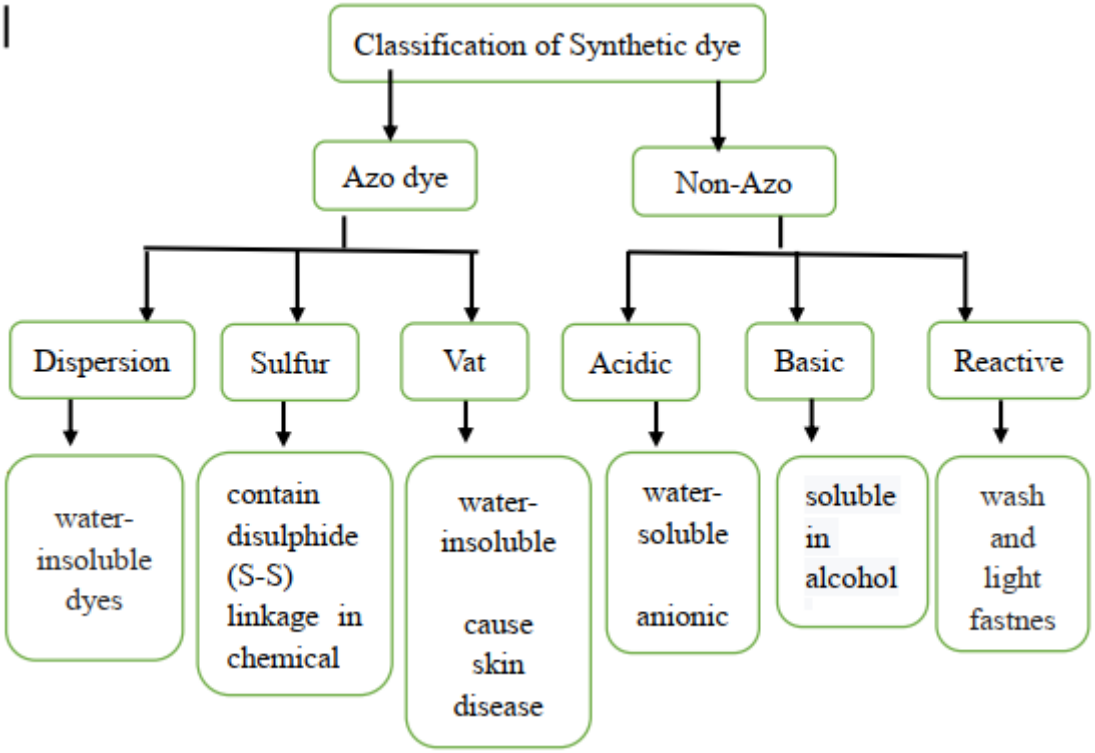

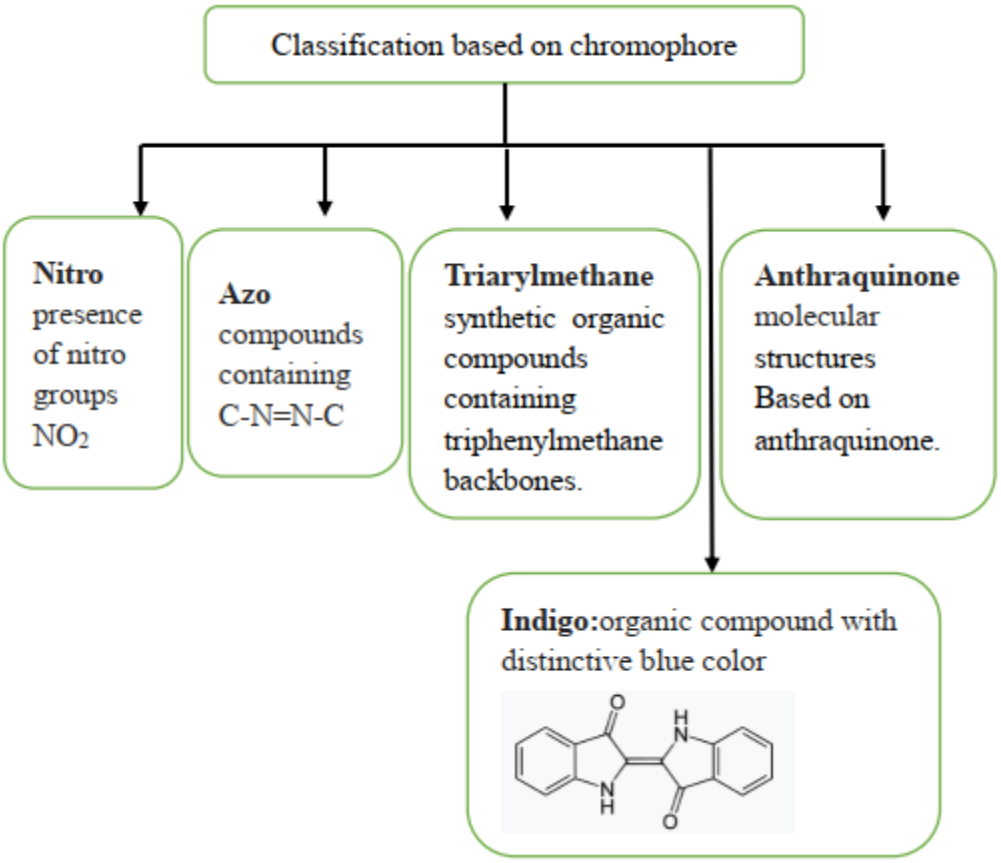

Figure 1.1 Classification of Dyes

1.1.3 Treatment of dye by advanced oxidation process (AOP)

Advanced Oxidation Process (AOPs) can directly mineralize or improve the biochemical properties of pollutants through oxidation process. It is based on the formation of highly active substances to oxidize a variety of pollutants. [18] These free radicals, especially hydroxyl radicals, are the main advantage of AOPs over conventional oxidation processes.

In this project, we use catalysts to generate electrons and holes under light. Then the photogenerated holes act as a strong oxidant to generate hydroxyl radicals OH* by reacting with water or electron donors like hydroxyl ions OH^-. Another free radical we used in this project is the reactive superoxide radical anions O_2^{-}*, which is generated by electron reduction of oxygen molecules.

1.2 Photocatalyst

This section reviews the different types of photocatalysts and the basic principles of photocatalysis. The first part compares the advantages and disadvantages of different types of photocatalysts, including metal-based photocatalysts and semiconductor-based photocatalysts. The necessary conditions of semiconductor as photocatalyst are also discussed. In the second part, the basic principles of the photocatalysis is described in detail, and common photocatalysts are introduced, with emphasis on TiO2 and ZnO.

1.2.1 Semiconductor-based photocatalysts

A good photocatalyst should be photoactive, able to harness the energy of visible and/or near-ultraviolet light, has high charge mobility and long charge carrier diffusion length, has strong catalytic activity, good stability, sustainability and low cost[19]. In the history of photocatalysis, many precious metals such as Pt, Rh, Pd, Ru, Ir have been used as photocatalysts [19-21]. However, although precious metals are less toxic than metal oxides and they are more harmful to the environment. In addition, due to the absence of bandgap and continuity of electronic states in the noble metal structure, photogenerated electron hole pairs are easily recombined, leading to the inactivation of the active sites and the reduction of photocatalytic efficiency. Therefore, metal oxides are more suitable for various applications of photocatalysts.

In recent years, TiO2, ZnO, CdSe, Fe2O3, ZnS and other semiconductor materials have attracted more and more attention as effective photocatalysts in the photocatalytic process due to their higher stability than metals and higher conductivity than insulators. Narrow bandgap is generally preferred over wide bandgap, since the minimum wavelength required to excite the electron-hole pair depends on the bandgap energy of the semiconductor photocatalyst, as shown in formula 1.1. Table 1.1 shows the bandgaps of some common semiconductor photocatalysts [22-24].

$$\lambda(nm) = \frac{hc\ (nm * eV)}{E_{bg}(eV)} \quad = \frac{1240\ (nm * eV)}{E_{bg}(eV)} \qquad (1.1)$$

Table 1.1 Bandgap of some common semiconductor photocatalysts.

Semiconductor-Based Photocatalysts	Bandgap Energy(eV)	Semiconductor-Based Photocatalysts	Bandgap Energy(eV)
ZnO	3.2	ZnFe2O4	1.9
WO3	2.7	ZnS	3.6
Fe2O3	2.2	CdS	2.4
TiO2	3.2	GaAs	1.4
SrTrO3	3.4	CdSe	1.7

In order for a semiconductor to be a good photocatalyst, not only the band gap but also the band edge position are critical. Figure 1.2 shows the band gap edge positions of a range of common semiconductor photocatalysts. [22-24]. The horizontal line shows the redox potential of H+/H2 and O2/H2O with normal hydrogen electrode (NHE). For the activity of semiconductor in photocatalytic reaction, the valence band of semiconductor should be in a more positive position than O2/H2O to have enough energy to generate OH radicals. At the same time, the conduction band should be more negative than H^-/H2 to reduce oxygen. In figure 1.2, the semiconductors that satisfied the edge requirement and suitable to be used as a good photocatalysts are TiO2, ZrO2, ZnO, ZnS and CdS.

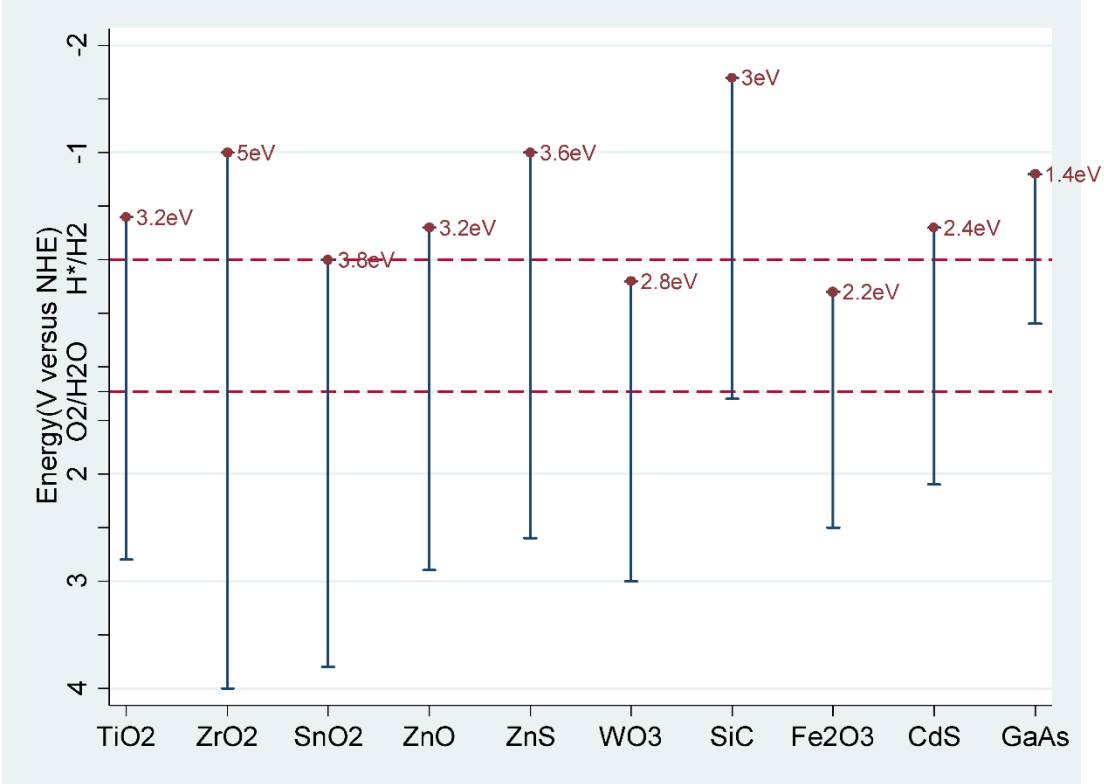

Figure 1.2 Band gap edge positions of common semiconductor photocatalysts [19]

However, the semiconductors that meet the band gap edge requirements are not all suitable to be used as photocatalyst. For example CdS is unstable in water, Fe2O3 is photocorrosion. Some photo-oxidation reactions have poor kinetics, such as WO3. In addition to high photoactivity, the ideal photocatalysts should be widely used and have low price.

Titanium dioxide is a widely studied photocatalyst with good stability and effective degradation of various organic dyes. [8,26] At the same time, zinc oxide, which has the same band gap as TiO2, is also characterized by high activity, strong oxidation ability, non-toxicity, good chemical stability, low cost and environmental friendliness. [23,27]. More importantly, ZnO nanostructures can be synthesized into many morphologies, including nanotubes, nanorods, nanoparticles and nanowires. These nanometer ZnO powders with large surface area have the potential to improve the degrade ability of catalysts, making ZnO a promising photocatalyst. Many experimental results have

shown that the photocatalytic activity of ZnO is even higher than that of many semiconductor catalysts, such as TiO2, ZrO2, CdS, Fe2O3 and WO3 [28-30]. In this project, zinc oxide was used as the main photocatalyst for dye degradation experiment.

1.2.2 Photocatalysts used in dye degradation

Semiconductor photocatalyst can generate free electrons and holes when it absorbed the photon energy equal to or higher than the band gap. (Described in Equation1.2).In semiconductor sensitized light reactions, several major processes occur with electron excitation. However, the carriers on the surface and interior of the photocatalyst can recombine, reducing the photocatalytic performance.

$$\text{Semiconductor Photocatalysts} + \text{hv} \rightarrow e^- + \text{h}^+ \qquad (1.2)$$

In an aqueous solution, an electric field spontaneously forms on the surface of the semiconductor. This electric field is caused by the difference in the liquid phase of the solution and the charge transfer caused by the potential of the solid semiconductor. [25][26]. The electron-hole pairs generated in this charge region are easily separated, causing electrons to migrate into the semiconductor. At the same time, holes will transfer to surface, producing active surface positions where the organic pollutants can be directly oxidized, resulting in photodegradation [23,25].

Different photocatalysts have different degradation ability on organic dye. Sobana, N., and M. Swaminathan[31] studied the photodegradation efficiencies of ZnO, TiO2 (anatase), ZnS, SnO2, Fe2O3 and CdS with an azo dye, acid red 18 (AR18). The result is shown in figure 1.3. We can see that SnO2, Fe2O3, CdS and ZnS showed really low degradation activity on AR18, probable due to their bandgap. The bandgap of SnO2 is 3.87 eV and ZnS is 3.6 eV, which are too large that the photon energy is not enough to generate free electrons and holes. CdS and Fe2O3 do have smaller bandgap, which are 2.4 and 2.3 eV separately. However, they are so small that the free carrier can quickly

recombine, impeding the degradation of the dye. It can also be seen from the figure that the degradation efficiency of ZnO is better than that of TiO2, which may be due to the larger surface area of ZnO (10 m2/g) than that of TiO2 (8.9 m2/g).

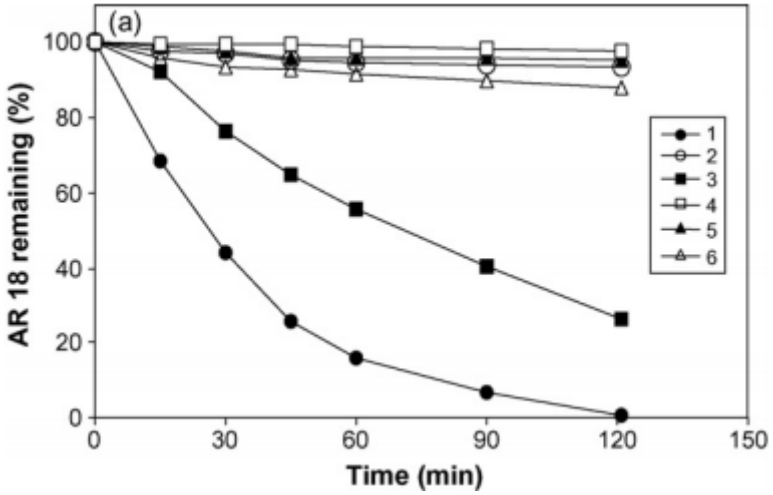

Figure 1.3 Effect of various photocatalysts on the degradation of AR18. [AR18] = 5 × 10−4 mol/L; pH 7.0 ± 0.1; amount of catalyst = 4 g/L; (1) ZnO (2) ZnS (3) TiO2 (anatase), (4) SnO2, (5) Fe2O3 and (6) CdS [31]

The particle morphology and microstructure of photocatalyst have a certain influence on the degradation ability of dyes. Xie, Juan, et al.[32] synthesized a series of ZnO particles with different morphologies shown in figure 1.4. Then photocatalytic activity of the samples were evaluated using methyl orange and the rugby-like ZnO photocatalyst showed the best performance.

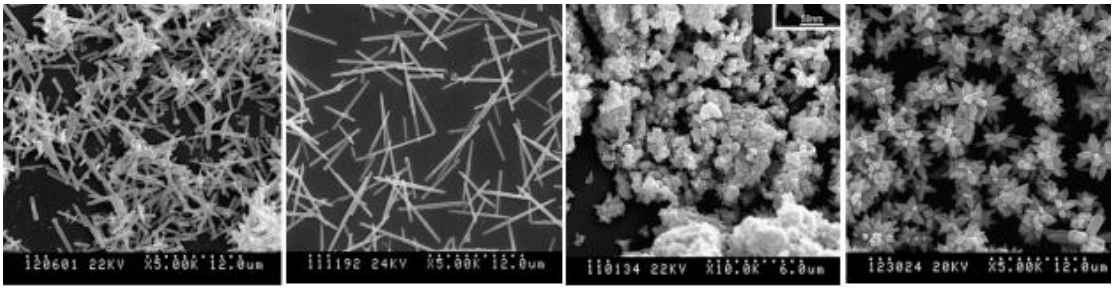

Figure 1.4 SEM images of ZnO particles prepared with different morphologies. (a) Rod-like; (b) Needle-like; (c) Rugby-like; (d) Flower-like [32]

Photocatalysts can degrade dyes in the form of composite materials and thin films. Danwittayakul, Supamas, Mayuree Jaisai, and Joydeep Dutta [33]synthesized oxide/zinc tin oxide (ZnO/ZTO) nanocomposites, tested its catalytic ability using methylene blue. Their result showed that ZnO/ZTO nanocomposite has better photocatalytic activity than original ZnO and is an attractive photocatalytic catalyst for solar energy. Siuleiman, Shahin, et al.[34]studied photocatalytic degradation of the organic azo-dye Orange II using TiO2 doped ZnO nanowire thin films and observed the good degradation ability of the prepared thin film. The ZnO nanowires array with TiO2 nanoparticles film on the top is shown in figure 1.5.

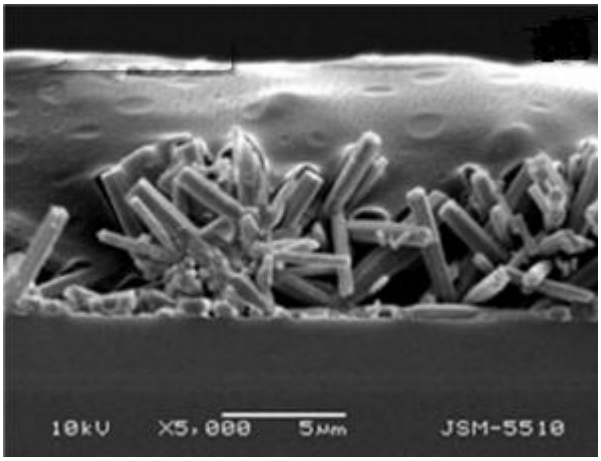

Figure 1.5 Films cross section–ZnO nanowires array with TiO2 nanoparticles film on the top. [34]

1.3 Nanomaterial

Nanomaterials are materials with an arbitrary one-dimensional scale of less than 100nm (1nm= $l0^{-9}$m). The basic units of nanomaterials can be divided into three categories according to their spatial dimensions. [35] a. Zero-dimensional nanomaterials (0D) refers to the spatial three-dimensional scale in the nanoscale, such as nanoparticles, atomic clusters, etc. b. One-dimensional nanomaterials (1D), such as nanowires and nanorods. c. Two-dimensional nanomaterial (2D) refers to the material with one dimension at the nanometer scale, such as ultra-thin film, multilayer film, etc.

Due to the particularity of size and structure, nanomaterials exhibt special physical effects: small size effect [36], surface effect [37], quantum size effect [38] and macro quantum tunneling effect [39].These four effects are the basic characteristics that make nanoparticles exhibit many strange physical and chemical properties, such as high strength, high thermal expansion coefficient, low melting point, abnormal conductivity and magnetization, strong wave absorption and high dispersion.

1.3.1 Properties

Surface plasmon resonance

The size of material has a great influence on its optical properties. One important reason for this effect is surface ionization resonance. Surface plasmon resonance (SRP) is the resonance oscillation of conducting electrons. When an incident light hits the interface of a material with positive and negative permittivity, these electrons are excited to resonate. The energy of surface plasmon resonance depends on the density of the free electrons and the medium around the nanoparticles. The resonance frequency of precious metals is within the range of visible light, so some gold nanoparticles appear red. Mie first solved Maxwell's equation for the interaction of light waves with metal surface in an electromagnetic field, and explained why gold nanoparticles appear red. [40]

As the particle size increases, the plasma beam redshifts and the wave width increases. For larger particles, the higher-order modes of light can no longer polarize nanoparticles evenly, so the peaks occur at lower energies. Figure 1.6 clearly shows the redshift and increase of wave width with the increase of nanoparticles.

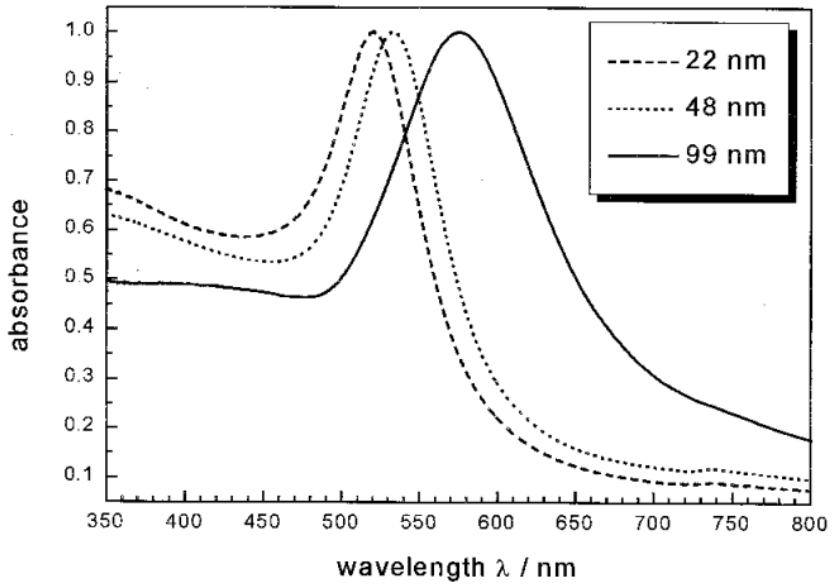

Figure 1.6 Optical absorption spectra of 22, 48 and 99 nm spherical gold nanoparticles.[41]

Quantum size effect

The special optical properties of nanomaterials may also be caused by the quantum size effect. When a single nanoparticle is smaller than the DE Broglie wavelength, electrons and holes are spatially limited, so electric dipoles can be generated and discrete levels of electron energy can be formed. Just like particles in a box, where the energy gap between adjacent energy levels increases as the dimension decreases. Figure 1.7 shows the energy levels of nanodots, nanowires and nanofilms. The electronic states of these nanomaterials are very different from their macroscopic counterparts. This change in states can lead to dramatic changes in the optical and electrical properties of materials.

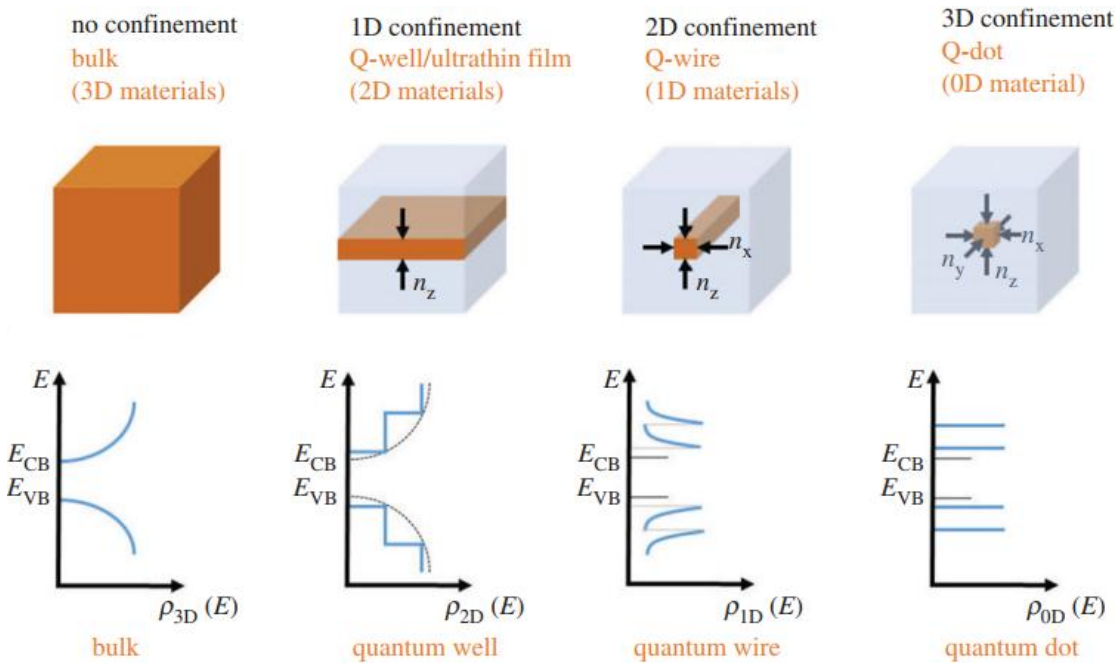

Figure 1.7 Schematic illustrating the density of states (DOS) in 1D, 2D and 3D confined materials.[42]

The quantum size effect is more pronounced in semiconductor nanomaterials. The reduced particle size increases the band gap, resulting in higher energy and higher frequency of interband transition. [43] In semiconductors, the interband transition need only a few electron volts, but it increases rapidly as the size decreases. For luminescence spectra, the peak shifts to higher energies as the particle size decreases. The correlation between such peaks and particle size is widely used to determine the size of nanoparticles.

1.3.2 Applications

Based on the special physical and chemical properties of nanomaterials and the rapid development of nanomaterials, nanomaterials are considered to have a broad application prospect in the fields of catalysis, environmental protection, new energy, optics, sensing, electronic materials, magnetic materials and biomimetic.

The application of nanotechnology is mainly based on the following aspects. First of

all, the special physical properties of nanomaterials. Like gold particles can be used as inorganic dyes to make stained glass. Gold nanoparticles can also show active catalytic ability.[44]Second, the large surface areas, such as photochemical cells made from porous titanium dioxide and sensors made from nanoparticles. What's more, ultra-small size make it possible to implement some functions. In molecular electronics, each molecule is used to control the transfer of electrons, making it possible to explore the supersize functions of electronic devices. When these molecules are biologically active, bioelectronic devices can be implemented.

Nanomaterials are mainly used in the field of photocatalysis as nano-semiconductor metal oxide[45]. Due to the large specific surface of nano-semiconductor metal oxide, it has a strong adsorption ability to the reactant, which effectively improves the interfacial charge transfer process, and enables photogenerated carriers to preferentially adsorb and react with the reactant, thus improving the photocatalytic efficiency. In addition, since semiconductor metal oxide nanomaterials have high surface energy and low melting point, they can react with reactants at low temperature, thus effectively avoiding the interference from other substances and improving the selectivity of photocatalytic reaction. Therefore, as a new type of photocatalyst, semiconductor nanometer metal oxide has become the research hotspot.

However, complicated preparation technology, high demand and high product cost have been bothering many scientists and restricting its application in practical production.[46-47] Ball milling is a simple, economical, high-yielding and practical method, which has been gradually recognized by people and is expected to solve the problem of nanomaterial industrialization

1.4 Planetary ball milling

High-energy ball milling is a method that use the rotation or vibration of hard balls to strike, grind, and stir the raw materials violently, and smash the powder into nano-

sized particles. Under the action of such strong force, a large number of vacancy, dislocation and other defects are accumulated in each layer, which makes the powder have higher lattice distortion energy and surface energy, making diffusion and reaction easier. Ball grinding can synthesize high melting point metals, alloys and composite materials which are difficult to obtain by conventional methods. It has been widely studied [46-47] for its simple process, low cost, high efficiency (kg products can be obtained at one time) and suitable for industrial production.

When grinding, we put powder into the grinding jar as well as the grinding ball, which is usually the same material of grinding jar. The grinding ball can be ceramic, steel or glass. The sample particles are affected by the collision between the ball and the vial wall. So controlling the exact size reduction through this path can be hard. In order to prevent contaminating the grinding powder, the material used for grinding jar and balls must be hard and strong, and not easily deformed.

1.4.1 Particles size with milling parameters

Grinding is a process of reducing the size of particles and is therefore known as a top-down approach. Grain size decreases with the increase of milling time. When the defect density in the local strain zone reaches the critical value, the grain begins to break due to the repeated deformation of the sample during the ball grinding process. This process is repeated over and over again, with grains becoming finer and finer until the nanostructure is formed. When the grinding time is extended to a certain extent, the fracture effect of strain on grain tends to be saturated, and the grain size remains at a certain value or even increase.

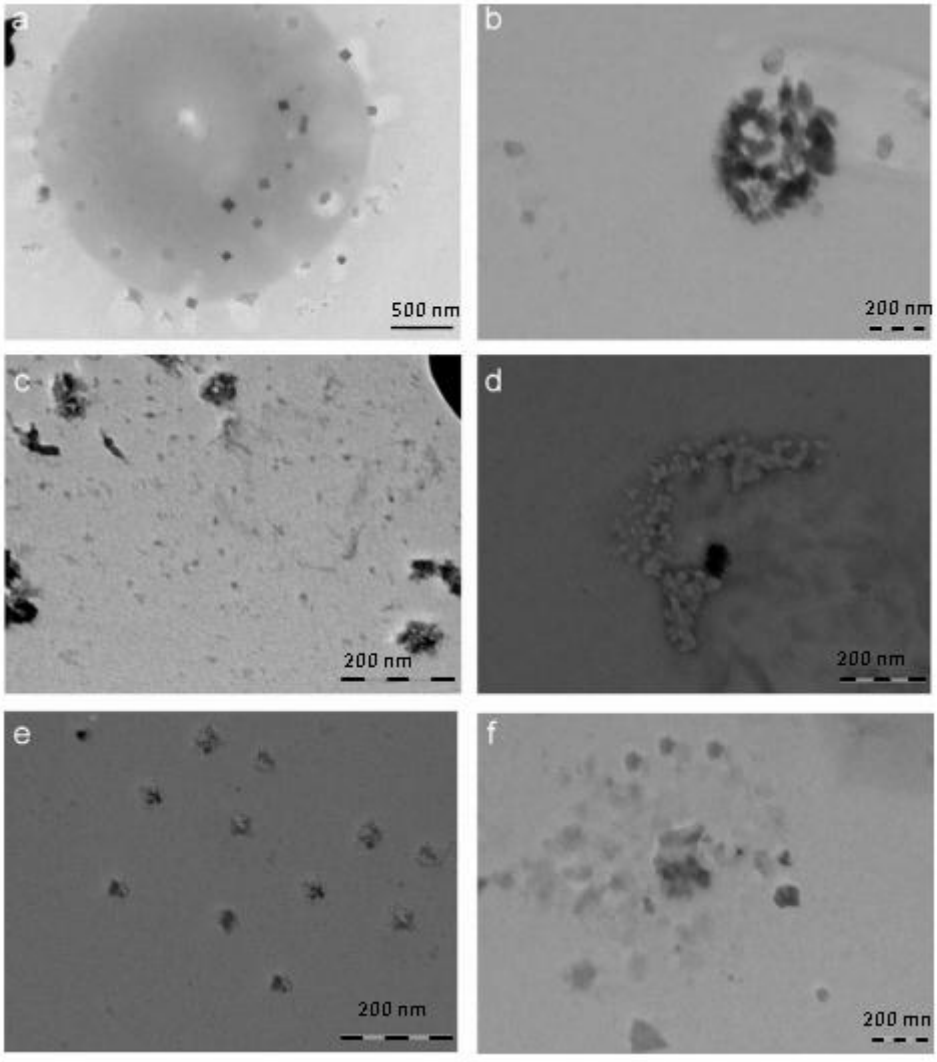

Figure 1.8 TEM micrographs of BaTiO3 nanoparticles produced by milling at the speed of 300 rpm for (a) 15, (b) 20, (c) 25, (d) 30, (e) 35 and (f) 40 h [48]

Nath, A. K., Chongtham Jiten, and K. Chandramani Singh[48] have researched the relationship of particle size with grinding time and the result was shown in figure 1.8. They grinded barium titanate (BaTiO3) from 15 to 40 hours at 300 rpm and used transmission electron microscope (TEM) to characterized the size. It can be seen that the average particle size of powder decrease from 48nm for 15 hours to 16nm for 25 hours. However, at 40 hours, the particle size increased from a minimum of 16 nm to 38 nm, due to the particle surface energy and microstrain.

Książek, K., et al. [49]studied the effect of planetary ball milling parameters on the

kinetics of thermal decomposition of CdCO3 and ZnCO3. Rasib, Siti Zalifah Md, and Zuhailawati Hussain [50]studied the speed influence of mechanical alloying of Fe-NbC composite and microstructure and properties of the product. Lyu, Honghong, et al. [51] researched the influences of ball milling on physical and chemical properties of carbon nanomaterials. As can be seen from figure 1.9, with the ball grinding time increasing from 0 to 12 hours, the specific surface area and the micropore volume of multiwall carbon nanotubes (MWNTs) increased significantly, while both decreased from 12 to 18 hours. This result suggested that MWNTs shortened with more pores under grinding with the increase of grinding time to 12 hours. After 12 hours of grinding, compaction and agglomeration effects may occur and the structure of MWNTs may be destroyed.

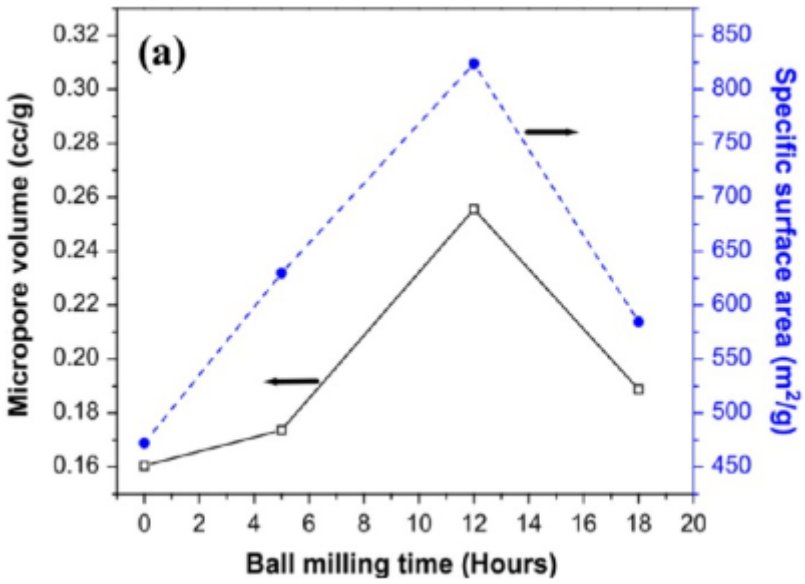

Figure 1.9 Effects of milling time on specific surface areas and micropore volumes of ball-milled multiwall carbon nanotubes (MWNTs) [51]

Planetary ball milling can also be used to prepare composites with better features or to achieve some special functions. Song, Myoung Youp, et al. [52] prepared the composite of Mg-Ni-Fe with good hydrogen-storage capacity using planetary ball milling at 250 rpm for 4 hours. Planetary ball milling helps by generating surface and interior defects in Mg which can act as active sites, also helps shorten the diffusion

distance of the hydrogen atom by reducing the particle size of magnesium. Planetary ball milling can be used to prepare conducting nanoparticle composites. Anno, H., et al. [53] conducted experiment to grind Bi powder with PANi solution at the speed of 600 rpm for 6 h to 12 h to prepare polyaniline (PANi)/Bi conducting nanocomposite. The advantage of ball milling method is that the Bi nanoparticles are prepared while the surface of the nanoparticles can be protected by PANi. Nanocomposites with good electrochemical properties can be prepared by planetary grinding. Wall, Clemens, et al.[54]used planetary ball milling to get LiF nanopowders and then used these nanopowders to prepare Co/LiF/C nanocomposites. They found that with longer gringing time, the crystallite size of LiF decreased, and electrochemical activity of Co/LiF/C increase when the composites are tested as cathode for lithium-ion-batteries. Figure 1.10 clearly shows the influence of grinding.

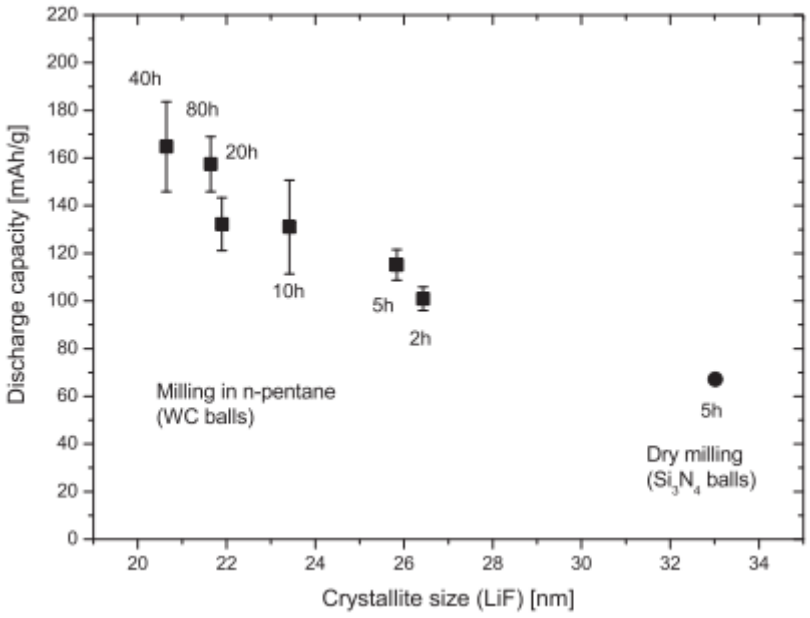

Figure 1.10 Influence of the crystallite size of LiF on the specific capacity of Co/LiF/C nanocomposites in the first discharge cycle. The LiF milling time is indicated at the corresponding data points.[54]

1.4.2 Photocatalyst manufacture

Planetary ball milling can be used to manufacture various types of photocatalysis with low cost and large scale. Zhu, Kaixing, et al. [55]prepared g-C3N4 thin nanosheets by planetary ball milling method and proved that the nanosheets had higher catalytic ability than the pristine bulk g-C3N4. Figure 1.11 shows the comparison of the size and layers between the bulk g- C3N4 particles and the grinded nanosheets. It can be seen that the size of pristine g-C3N4 is over 2 μm with multiple layers as shown in Fig.1.11a inset. After grinding, the TEM image shows transparent feature, indicating ultrathin layers of nanosheet with one or two atoms.

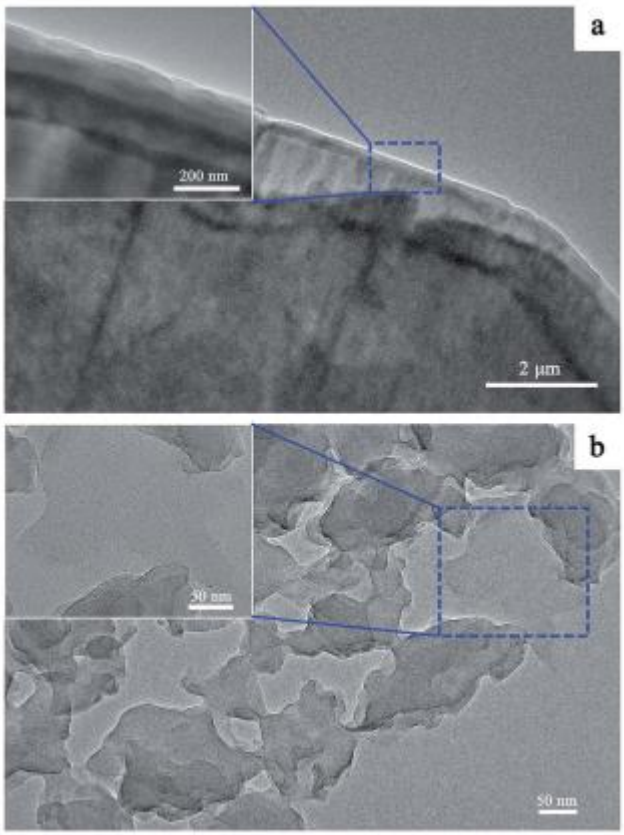

Figure 1.11 TEM images of a pristine g-C3N4 particle (a) and nanosheets (b) Inset shows the enlarged part within the dash lines [55]

One good reason to use planetary ball milling is that the structural stability of samples will be maintained after milling process. Hassani, Aydin, et al. [56] prepared magnetite

(Fe3O4) nanoparticles for 6 hours. They did XRD analysis to compare the patterns of unmilled magnetite sample and nanoparticles with 6 hours milling. As can be seen from figure 1.12, the XRD pattern of the unmilled magnetite sample is similar to the XRD pattern of magnetite nanoparticles after the ball-milled process. It proved that structural stability of primary magnetite was maintained.

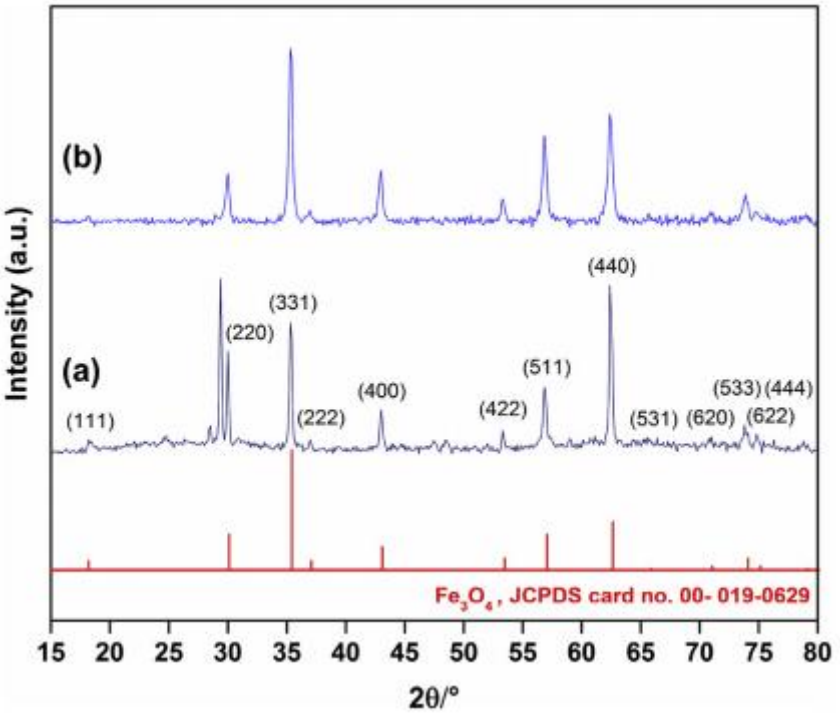

Figure 1.12 XRD pattern of (a) unmilled magnetite sample and (b) magnetite nanoparticles after 6 h ball milling[56]

Another advantage to use planetary ball milling is that it is a nice way to synthesis nano-photocatalysts with large surface area and tunable particle size. Using planetary ball milling can also help band-gap engineering and improve the efficiency of electron transfer. All those properties contribute to improving the photocatalytic ability of the material.

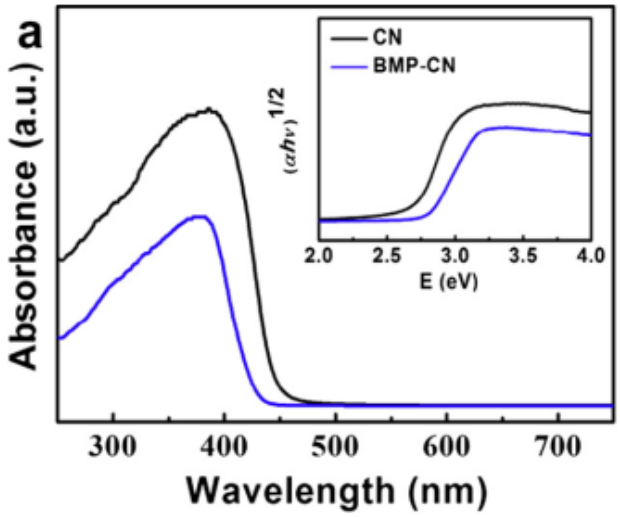

Figure 1.13 UV–vis diffuse reflectance spectra (DRS) of g-C3N4 powder (CN)and ball milling process g-C3N4 powder (BMP-CN)[59]

Taking photocatalyst C3N4 as an example. Previously, people have to use template to fabricate g-C3N4.[57][58] However, the template may either not be environmentally friendly or introduce impurities that prevent the photodegradation process. Cai, Qifeng, et al.[59] used ball milling to prepare nanoporous g-C3N4 with no template. They used UV–vis diffuse reflectance spectra (DRS) to compare the optical properties of the samples. (Figure 1.13) For the original g-C3N4 powder, the absorption edge rising at 460 nm, which is related to its 2.7 eV band gap. The results show that the absorption edge of g- C3N4 powder is blue shifted during ball grinding. This indicates that the increase of band gap is beneficial to the enhancement of photocatalytic activity. In addition to band gap engineering, they also found that grinding improves the efficiency of the electron transfer process. They analyzed the photocurrent of g-C3N4 powder (CN) and ball milling process g-C3N4 powder (BMP-CN) under visible light illumination during on–off cycles. It can be seen from figure 1.14 that the electrode using ball milling process g-C3N4 powder revealed higher transient photocurrent. This improved separation efficiency of photo-generated electrons and holes is helpful to improve dye degradation process.

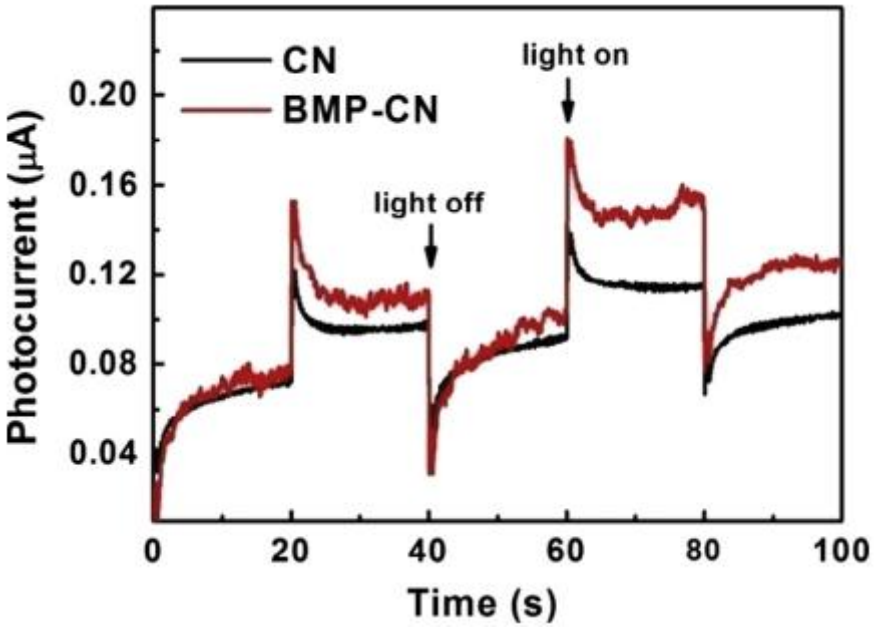

Figure 1.14 Photocurrent–time profiles of g-C3N4 powder (CN) and ball milling process g-C3N4 powder (BMP-CN) under visible light illumination (k > 420 nm).[59]

Planetary ball milling can be used in doping to improve the photocatalytic ability of nanomaterials. Some doping material like Fe-doped TiO2 proved to have a better photocatalytic efficiency than TiO2 alone. Various elements were introduced into its crystal structure to change the band gap of titanium dioxide. Planetary ball milling provides an effective and simple method for mass production of materials. Carneiro, J. O., et al.[60]conducted experiments grinding TiO2 and Fe powder for 5 hour at the speed varying from 250 to 350 rpm. They used 5 mg/L Rhodamine B (Rh-B) to measure the degradation ability of samples. Figure 1.15 shows the result of photocatalytic efficiency. It can be seen that Fe-doped TiO2/milled at 350 rpm has the best photocatalytic ability.

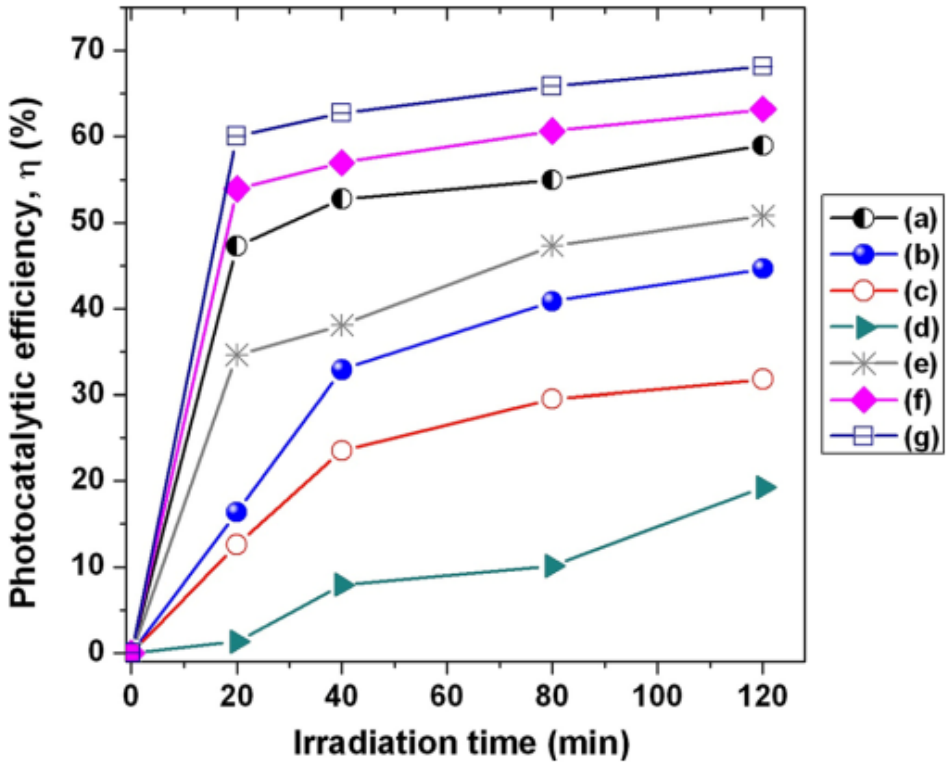

Figure 1.15 Photocatalytic degradation, over time, of Rh-B aqueous solution in the presence of TiO2-based pressed disk samples containing: a undoped TiO2/without milling, b undoped TiO2 milled @ 250 rpm/, c undoped TiO2/milled @ 300 rpm, d undoped TiO2/ milled @ 350 rpm e Fe-doped TiO2/milled @ 250 rpm, f Fe-doped TiO2/milled @ 300 rpm, and g Fe-doped TiO2/milled @ 350 rpm [60]

Planetary ball milling method can also be used in ZnO band gap engineering. Choi, Young In, et al.[61]used wet and dry ball-milling method to hybridize Ag with ZnO nanoparticles, and examined their photocatalytic properties. They proved that ball milling can engineer the band gap of ZnO and enhance the visible light absorption of ZnO. Reddy, I. Neelakanta, et al. [62] prepared Fe doped ZnO nanoparticles by ball milling method and evaluated the photocatalytic efficiency by degradation of methylene orange (MO) dye in aqueous solution under sunlight irradiation. Figure 1.16 (a) showed that the MO absorbance decreases slowly with the increase of light irradiation time. (b) showed 40 hours ball milled Fe doped ZnO nanoparticle have better dye degradation ability than undoped ZnO.

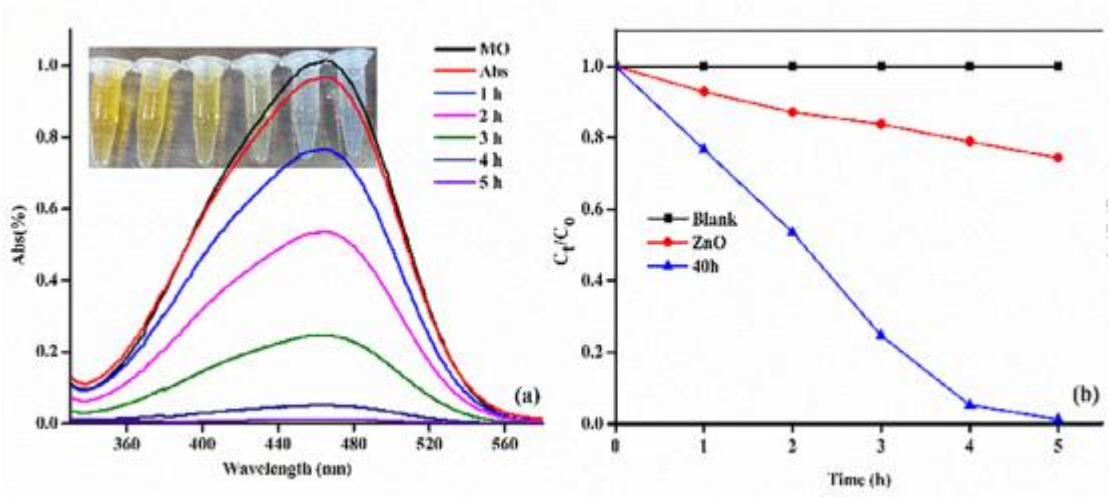

Figure 1.16 Photocatalytic degradation of methylene orange (MO) aqueous solution under sunlight irradiation (a) Absorption spectra of MO solution sampled at various irradiation time using 40 h ball milled Fe doped ZnO nanoparticle, (b) Photocatalytic activities of blank test(no light), ZnO and 40 h ball milled Fe doped ZnO nanoparticle [62]

1.4.3 Machine used in this project and grinding mechanism

The planetary mill used in this study is Pulverisette 7, Fritsch horizontal planetary ball mill made by Fritsch GmbH, Germany. Its vial is made of Si Nitride and the volume is 80mL. And its grinding speed can reach 1100 rpm. [63] The grinding beads made of Zirconia (2 mm or 3mm in diameter) and can be placed inside the vials with the samples and together for grinding at setting time and speed. It can be used for dry grinding, but we usually grind with different solvent for desired grinding results.

Figure 1.17 Fritsch pulverisette-7 planetary ball mill [63]

The raw material is crushed and grinded by grinding beads in the grinding bowl. There are two kinds of centrifugal forces, one from grinding bowl rotating around its own axis, and the other from the rotating main disc. Since these two rotations are in opposite directions, the centrifugal force alternatively act in same and opposite directions.[64] This has a great effect on the grinding beads, which have two kinds of motion: one is the rotational motion around the axis of the main disk, and the other is the planetary motion around the axis of the bowl. So the friction and collision between the ball and the bowl will grind the ingredients to the required size.

This grinding machine can be used in both wet and dry grinding mode. Wet grinding method is used in this project because it is beneficial over dry grinding process. Dry grinding can cause a lot of damage to the inner wall of the grinding bowl and beads, which may lead to contamination to grinding materials. For wet grinding, if the grinding speed, time and other parameters are set correctly, there will be less collision and pollution.

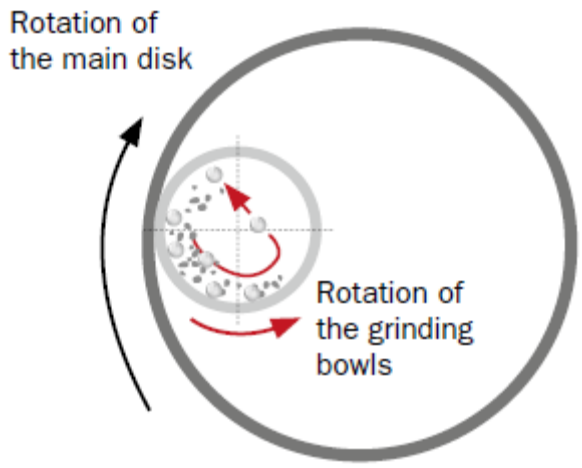

Figure 1.18 Basic schematic of planetary ball mill [63](The arrow in the jar shows the direction of centrifugal force)

The crushing of raw material is mainly carried out by high-energy impact of grinding beads. While the machine is operating, the main disc rotates toward one direction(for example clockwise), while the grinding bowl with solvents and beads are rotated around its axis (for example counterclockwise), which is opposite to main disc. The details are shown in figure 1.18. The superposition of centrifugal force makes the grinding beads to move along and rebound from the inner wall of the grinding bowl. At a certain point in the rotation, the competing centrifugal forces of main disc and grinding bowl cancel each other out. The grinding beads then leave the bowl wall and collide with the wall on the other side. This diagonal travel through the bowl will hold extremely high speed and generate both heat and mechanical energy that can grind the sample.

1.5 Objectives and overview

The main objective of this project is to prepare ZnO nanoparticles using planetary ball milling method and apply them to remove the organic contaminants in water.

1.5.1 The specific objectives

1. To prepare ZnO nanoparticles using planetary ball mill and study the effect of the grinding conditions on the particle size of the produced nanoparticles.

2. To research the methodologies of dye degradation using prepared semiconductor ZnO nanoparticles.

3. To design experiment set up and follow the procedure to conduct dye degradation experiments, study on different parameters that can affect the result of the experiment.

4. To evaluate the photocatalytic activity of ZnO with different particle size, study on how those grinding parameters can affect the photocatalytic ability of ZnO.

1.5.2 Report outline

In this project, the ZnO photocatalysts were prepared using planetary ball milling method and used for degradation of organic dye. Chapter 1 presents a comprehensive literature review on textile dye, nanomaterial, semiconductor-based photocatalysts as well as the machine used in this project and its grinding mechanism. Chapter 2 discusses the photodegradation reaction mechanism including bromophenol blue degrade mechanism and parameters that influence photodegradation. Chapter 3 is focused on using high energy ball milling method to prepare nanosize ZnO catalysts with different size. Then the setup and procedure of dye degradation experiments were introduced and the experimental results were analyzed. Chapter 4 discusses the results of this project and outlines potential future work.

Chapter 2 Photodegradation Methodologies

In this chapter, a comprehensive review will be presented on the photodegradation reaction mechanism and the discussion of main parameters that influence photodegradation. In the first part, ZnO crystal structure and catalytic performance will be described in detail. The second part discusses the photodegradation reaction mechanism, which include electron-hole pairs generation, charge-carriers reaction and degradation of dye compounds. The third part analyzes different parameters that affect the dye degradation efficiency.

2.1 Photocatalyst and dye

This section presents the properties of photocatalyst and dye which are going to be used in the experiment in this project. In the first part, the three crystal structures and properties including photocorrosion of ZnO will be described in detail, following the factors that affect the ZnO photocatalytic properties. The second part focuses on the photodegradation mechanisms of bromophenol blue and how to prepare BPB stock solution for the experiment.

2.1.1 ZnO catalytic performance

Zinc oxide (ZnO) is an II-VI direct semiconductor with the band gap width of 3.2 eV (near ultraviolet range). The exciton binding energy is as large as 60mev at 300 K. [64]Since the defects especially oxygen vacancy in different ZnO samples are different, the values of band gap energy may not be exactly the same in different literatures.

There are three crystal structures for ZnO: Rock-salt cubic, hexagonal wurtzite and cubic zinc blende. The structure of rock-salt crystal[65](Figure 2.1 (a)) can only exist under relatively high pressures around 10GPa. Cubic zinc blende-type structure (Figure 2.1 (b)) can only grow epitaxially on the substrates with cubic lattice structure. Wurtzite crystals(Figure 2.1 (c)) have the most compact atomic arrangement. Each Zn atom is

located in a tetrahedron formed by four adjacent O atoms, forming a regular tetrahedron. Similarly, each O atom has four adjacent Zn atoms, which are also tetrahedrons. This tetrahedral coordination pattern leads to the asymmetric structure of ZnO. It shows that ZnO lattice origin point is not symmetric center, which leads to unique piezoelectric and thermoelectric properties. Wurtzite structure is the most stable structure of the three, so nearly all photocatalytic studies are focused on this structure.

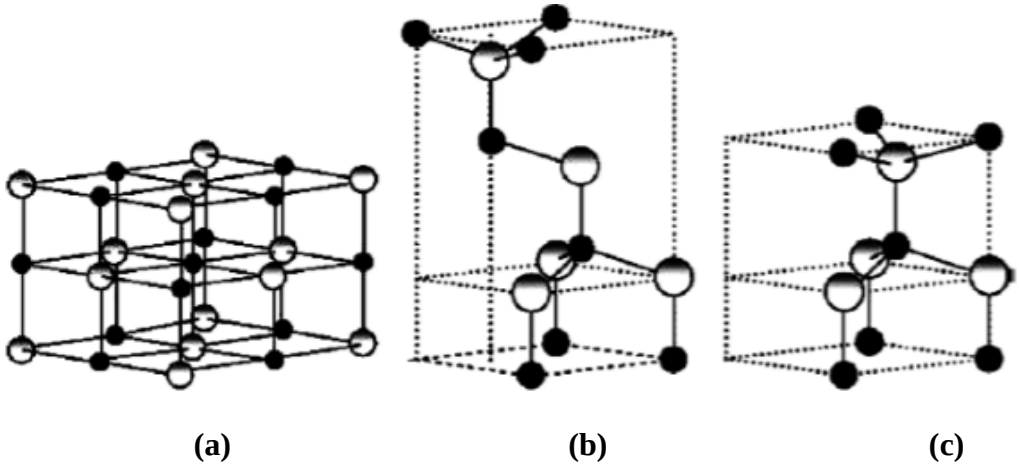

Figure 2.1 Crystal structures for ZnO. (a)Rock-salt (b) Zinc blende (c) Hexagonal wurtzite.[65]

There are many factors that can affect the photocatalytic properties of zinc oxide. In the process of crystal formation, there are many variables such as temperature, atomic movement and lattice defects that can affect the internal structure of the crystal lattice defects and surface area, which will influence the crystal light capture efficiency and absorption ability of pollutants. What is more, the morphology of ZnO also have important influence on photocatalytic properties. Morphology influence mainly caused by the shape of a semiconductor, grain size, porosity, specific surface area of catalyst, the surface reaction activity sites and so on.

ZnO is not really stable under illumination and can react with photogenerated holes to form Zn^{2+}, resulting in photocorrosion.[66]

$$\mathrm{ZnO} + 2h^{+} \rightarrow Zn^{2+} + 0.5O_2 \qquad (2.1)$$

In acid or alkaline environment, ZnO will have further corrosion reaction under light.

$$\mathrm{ZnO} + 2H^{+} \rightarrow Zn^{2+} + H_2O \qquad (2.2)$$

$$\mathrm{ZnO} + 2OH^{-} + H_2O \rightarrow Zn(OH)_4^{2-} \qquad (2.3)$$

Despite these shortcomings, ZnO still has advantages over other semiconductor photocatalytic materials. For example, the photodegradation rate of ZnO is higher than many other catalysts. What is more, ZnO shows a better degradation effect on different organic dye wastewater.

2.1.2 Bromophenol blue degradation mechanism

Bromophenol Blue (C19H10Br4O5S) belongs among the type of triphenylmethane dye. This type of triphenylmethane dye belongs to the three most widely used synthetic dye types. It has certain toxicity and resistant to biodegradation, which can inhibit the growth of most biological species. The Bromophenol Blue (BPB) dye is widely used in textile, biological dyeing, veterinary medicine and other industrial fields. The basic molecular structure is three benzene ring connected to the same carbon atom (see Fig. 2.2). This particular chemical structure is relatively stable and very difficult to be degraded by ordinary microorganisms. Therefore, when the dye molecules are discharged with wastewater, it can cause serious pollution to the environment.

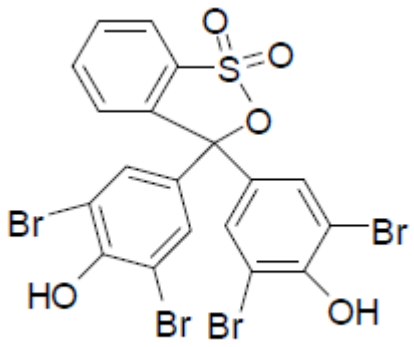

Figure 2.2 Molecular structure of Bromophenol Blue (BPB)

BPB was chosen to be a representative industrial dye to be degrade in this project due to several reasons. BPB dye is a common type of dye for industrial use and has excellent fastness against washing. At the same time, the degradation of BPB has rarely been studied by other researchers under similiar conditions.

Degraded by photocatalysts, the main degradation products are phenol, ammonium and sulfate. Figure 2.3 shows one of the photodegradation pathways of bromophenol blue. [67]

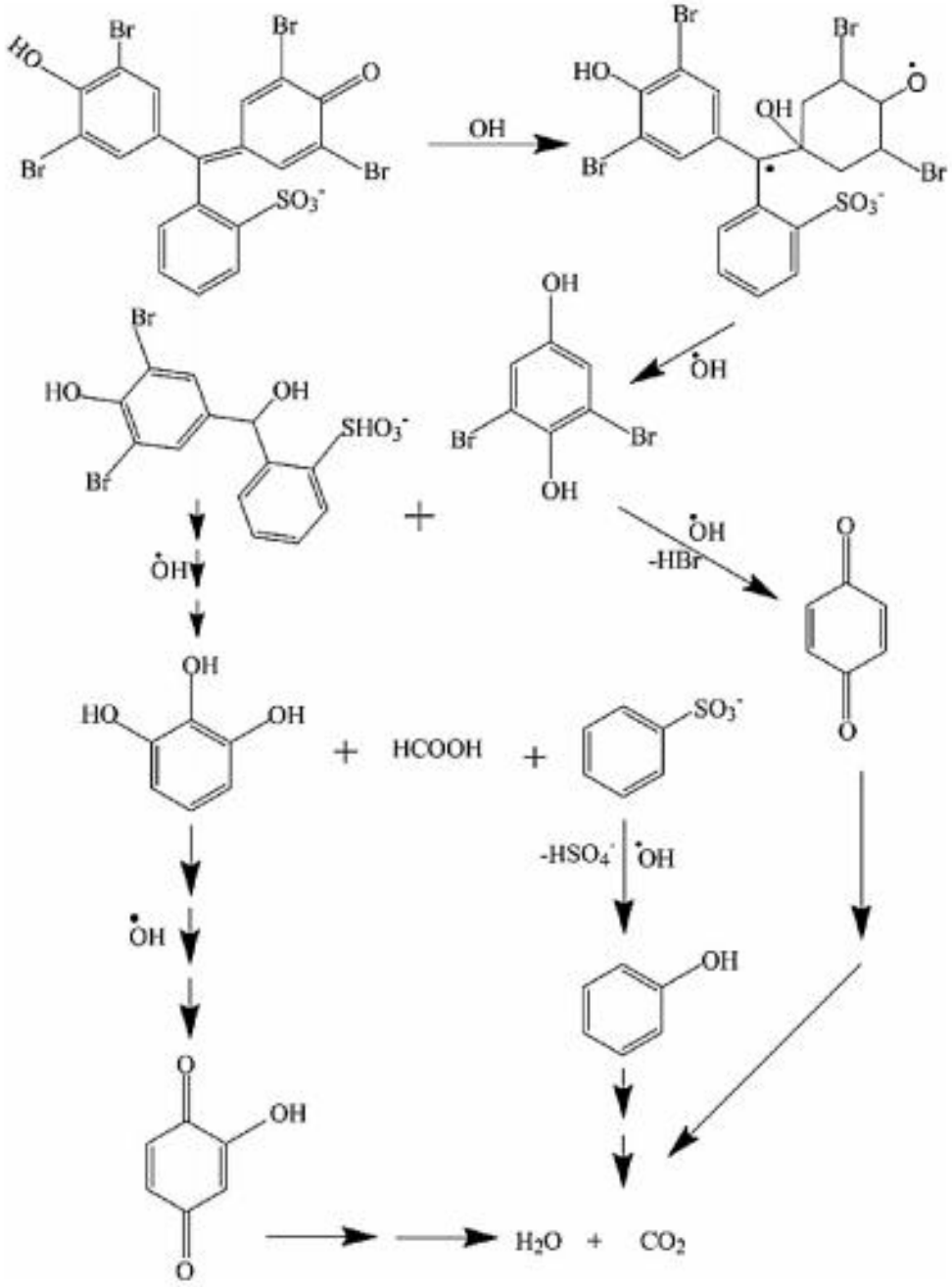

Figure 2.3 Reaction pathway for degradation of BPB [67]

Bromophenol blue powders (stock code 01326) used in this project was purchased from the science store in University of Victoria. Using the powder, we prepared 12 ppm and 7 ppm BPB stock solution for dye degradation experiments. The details of preparation process is presented in section 3.3.

2.2 Photodegradation reaction mechanism

The photocatalytic process can be divided into three big steps: First of all, electron-hole pairs generation. When light irradiates on ZnO, it will absorb photons with energy same or greater than the band gap. As a result, electrons in the valence band will be excited and travel through the forbidden zone to the conduction band. At this time, strong oxidizing hole h^+ will appear in the valence band. Next step, the strong oxidizing hole h^+ will oxidize the hydroxyl group and water molecules on the surface of ZnO into radical OH*. Last step, the free radical OH*, as a strong oxidant, diffuses around the pollutants and oxidize these organic pollutants into water, carbon dioxide or other harmless substances. The mechanism of photocatalytic oxidation on the surface of photocatalyst nanometer ZnO by electron-hole pairs is shown in figure 2.4.

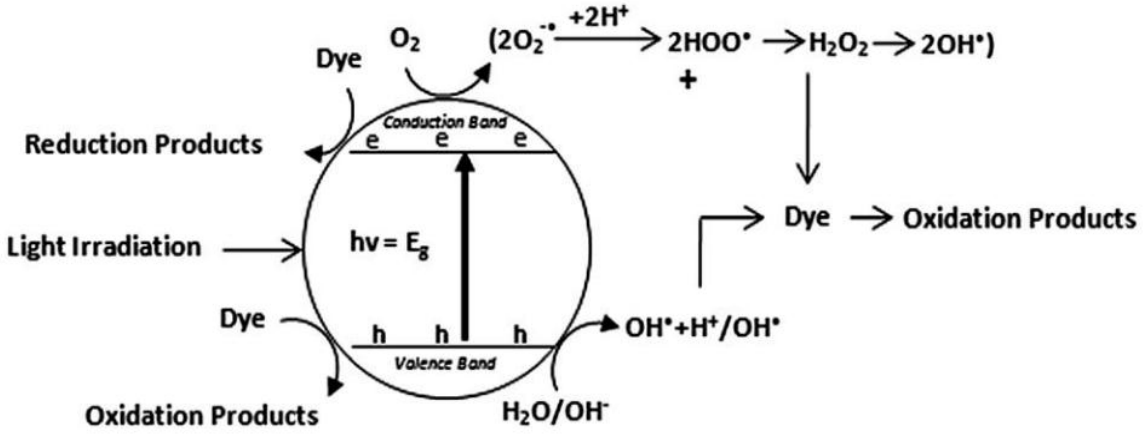

Figure 2.4 Mechanism of photocatalytic oxidation on the surface of ZnO [68]

2.2.1 Electron-hole pairs generation

Photocatalytic reaction starts from the transition of photonic electrons of semiconductor catalyst under irradiation. Electrons in the valence band are excited and travel through the forbidden zone to the conduction band. Holes with strong oxidation ability are left on valance band. The generation result of electron hole pair is shown in

the following formula 2.4

$$\mathrm{ZnO} + \mathrm{hv}(\lambda < 380\ \mathrm{nm}) \rightarrow ZnO\left(e^{-}(CB) + h^{+}(VB)\right) \quad (2.4)$$

2.2.2 Charge-carriers reaction

Before the electron-hole pairs recombine, they can react with different scavengers to generate oxidant. On valance band, the positive holes are strong oxidant themselves and can directly oxidize the pollutants around. They can react with hydroxyl ions or water molecules to generate hydroxyl radical OH* (See formula 2.5, 2.6). The OH* radicals generated on the surface of ZnO are extremely powerful oxidant and can nonselectively react with adsorbed organic dye molecules.

$$h^{+} + H_2O \rightarrow OH* + H^{+} \quad (2.5)$$

$$h^{+} + OH^{-} \rightarrow OH* \quad (2.6)$$

At the same time, the photogenerated electrons on conduction band will be trapped by molecular oxygen and reactive superoxide radical anions O_2^-* will be produced. Other oxidants may also be produced like hydroperoxyl radicals HO_2*, hydroxyl radical OH* as well as hydrogen peroxide H_2O_2. The related formulas are shown below.

$$O_2 + e^{-} \rightarrow O_2^{-}* \quad (2.7)$$

$$O_2^{-}* + H^{+} \rightarrow HO_2* \quad (2.8)$$

$$HO_2* + e^{-} + H^{+} \rightarrow H_2O_2 \quad (2.9)$$

These oxidants of hydroperoxyl radicals HO_2* and hydrogen peroxide H_2O_2 will take part in further oxidation process and more hydroxyl radicals OH* will be generated, as

shown below.

$$O_2^- * + H_2O \rightarrow HO_2 * + O_2 + OH^- \quad (2.10)$$

$$H_2O_2 + e^- \rightarrow OH * + OH^- \quad (2.11)$$

$$H_2O_2 + O_2^- * \rightarrow OH * + OH^- + O_2 \quad (2.12)$$

$$H_2O_2 + \text{hv} \rightarrow 2OH * \quad (2.13)$$

As the process of electron-hole pairs react with molecules around and generate oxidants, these electron-hole pairs are also recombine and release heat. The efficiency of recombination are greatly affected by ZnO defects especially bulk defect, which will be discussed in next section.

$$ZnO\ (e^- + h^+) \rightarrow ZnO + heat \quad (2.14)$$

2.2.3 Degradation of dye compounds

Free radicals of HO_2*, O_2^- *, OH* and photogenerated holes (h^+) with high oxidize ability will continually react with the dye molecules around and completely mineralize them into water, carbon dioxide and other harmless substances, shown in the following formulas.

$$\text{Dye} + OH * \rightarrow CO_2 + H_2O + intermediates \quad (2.15)$$

$$\text{Dye} + h^+(VB) \rightarrow oxidation\ products \quad (2.16)$$

$$Dye + HO_2 * + O_2 \rightarrow CO_2 + H_2O \quad (2.17)$$

2.3 Parameters that influence photodegradation

Many parameters can affect the photocatalytic ability of ZnO, including crystal structure, surface area (particle size), morphology, defects, etc. The first section presents the effect of particle size and surface area on photodegradation efficiency. The second and third sections focus on the influence of defects because they largely affect the generation, transfer and recombination of photogenerated carriers. How the type and location of different defects may lead to improvement or deterioration of photocatalytic activity will be presented in details. The last section discusses the influence of ultrasonic to dye degradation.

2.3.1 Effect of surface area

Particle size is an important parameter affecting the photodegradation efficiency. It is well known that when particle size decreases, surface area per unit volume increases. At the same time, the number of dispersed particles per volume in the solution increases. Since degradation reactions occur on the surface of catalysts, it is necessary to understand the influence of particle size and surface area on photodegradation efficiency.

Generally speaking, photocatalytic activity is considered to be determined by the catalysts ability of light absorption, carrier separation and carrier transfer efficiency. Surface area of catalysts can largely affect (increase in most cases) the transfer of carriers and free radicals. When other factors including lattice defects are the same, the increasing of surface area will lead to the increasing of photocatalyst activity. The main reasons are discussed below.

Due to the surface effect, when the particle size is smaller, the more particles per unit mass and larger size of surface area. The size of surface area is an important factor to

determine the adsorption capacity and active center of the catalyst. For general photocatalytic reactions under the condition of sufficient reactants, when the active center density on the catalyst surface is constant, the larger the surface area, the more OH^- can be adsorbed, and the more highly active $OH*$ can be generated, thus improving the catalytic oxidation efficiency.

Carrier transfer efficiency is greatly affected by particle size. It can be seen from the diffusion equation (Equation 2.18) [69]that the time for the electron or hole to reach the surface is proportional to the square of the particle radius. In equation (2.18), r is radius of nanoparticle sphere. D is Diffusion coefficient ($D_{e^-} = 2 * 10^{-2}\, cm^2/s$). [69] The smaller the particle, the shorter the time needed for photogenerated electrons and holes to reach the surface. This short time of transfer means higher probability of photo-carriers reaching the surface, which leads to higher concentration of electrons and holes on surface. This higher concentration of free photo-carriers increase the possibility of them to be captured by surface adsorbed reactants, which cause higher photocatalytic activity. The random walk model is applied to describe the motion of free electrons and holes. The average transit time from the particle interior to the surface is:

$$\tau = \frac{r^2}{\pi^2 D} \qquad (2.18)$$

According to the calculation, for ZnO particle size of 1 micron, it takes 10^{-7}second for electrons to transfer from the body to the surface. However, it only need 10^{-11}second for electrons to transfer in the same kind of ZnO with particle size of 10nm.

2.3.2 Effect of bulk defect

As an inherent structure, defects exist widely in zinc oxide. Therefore, it is of great importance to study the effect of defects on ZnO photocatalytic properties. The bulk defects are defects that exist in the structure of ZnO lattice. This kind of defects can act as recombination center and capture photogenerated carriers, which will reduce the

concentration of electrons and holes in the surface [69] and thus reduce the photocatalytic efficiency.

One of the possible mechanisms of how the bulk defects influence the photocatalytic process is shown in figure 2.5. Under the irradiation of light, the excitation electrons will transfer to the conduction band and react with O_2 to generate superoxide radical anions ($O_2^- *$). The holes in the valence band will react with OH^- to generate hydroxyl radicals. The bulk defects (dots between CB and VB) act as recombination center, in which the photogenerated electrons and holes will recombine. The existence of recombination centers will greatly affect separation and transfer efficiency of photo-carriers.

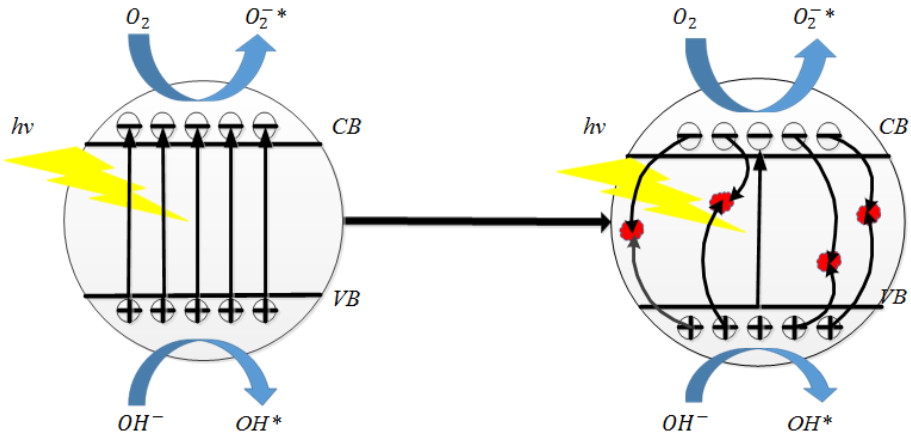

Figure 2.5 Influence of bulk defects to photocatalytic process

In this project, ZnO photocatalysts was prepared by planetary ball milling. This ball milling method may cause the damage of the crystal structure of bulk ZnO. Many deep level defects may appear in prepared photocatalysts, and those bulk defects may include zinc interstitial (Zni), oxygen interstitial (Oi), zinc vacancy (VZn), oxygen vacancy (VO) and antisite oxygen (OZn) [69-71].

To understand whether our ball milling method affect the catalytic ability of ZnO or

not, it is needed to design experiments using pristine bulk ZnO and grinded ZnO. To research how this grinding affect the catalytic ability of ZnO, it is necessary to do dye degradation experiments using grinded ZnO with different grinding parameters (speed and time).

2.3.3 Effect of surface defect

Since defects play an important role in photocatalyst degradation of dyes, it is necessary to identify the impact of different types of defects. According to the location of defects, they can be divided into surface defects and bulk defects [72-73]. We know from the last section that bulk defects are often considered as recombination centers, leading to the deterioration of photocatalytic activity. However, the surface defects act as active areas and can be beneficial to the photocatalytic activity.

Surface defects refer to the superficial defects on the surface of catalyst particles. They would also capture photogenerated carries, but unlike bulk defect, these photogenerated electrons and hole are quickly released. More importantly, surface defects can absorb O_2 and organic pollution molecules. This absorbed O_2 can quickly react with photogenerated electrons to form superoxide radicals and degrade the absorbed dye molecules. Therefore, surface defects not only increase the number of active spots, but also accelerate the reaction of dye degradation.

ZnO with surface defects can be synthesized through many ways including vacuum de-oxygen, high temperature quenching for oxygen vacancies and hydrogen reduction possess [72,74]. Those catalysts with surface defects all showed higher photocatalysts performance.

In chapter 3, we will try to grind pristine ZnO by hand in N_2 environment instead of air to make catalysts with surface defects. This defects may related to oxygen vacancy, which may help enhance photocatalytic activity. Chapter 3 will also present the details

about dye degradation experiments and the photocatalytic performance of different ZnO catalysts.

2.3.4 Effect of sonication

In the dye degradation experiment, there is an ultrasonic process. During this process, ultrasound may cause decolorization, affecting the performance of photocatalysts.

The principle of ultrasonic radiation degradation originates from the high energy of ultrasonic radiation. The sound energy will generate many small specific areas with high temperature ranging from 1900 to 5200K and high pressure exceeding 50MPa. [75] Water molecules in these specific areas will decompose to oxide and help to degrade organic dye.

Whether ultrasonic can degrade organic dye in a short time depends not only on the stability of dye, but also on the level of ultrasonic powder. In order to evaluate the photodegradation ability of different catalysts, it is important to know the effect of sonication in the experiment.

Chapter 3 Experiments and Results

This chapter presents the general procedure of experiment and shows the results of dye degradation reactions using different ZnO catalysts. First section introduces the way to use planetary ball mill to prepare ZnO nanoparticles. Section 3.2 presents the dye degradation experiment set up and the preparation of catalyst powders from previous suspension. Section 3.3 introduces the procedure of experiments, focusing on the control experiment and adsorption study. The last section presents the degradation result of ZnO with different particle sizes

3.1 Synthesis ZnO nanoparticles

To synthesis the nanoparticles of the photocatalyst, we grind the bulk ZnO using planetary ball mill. The first part talks about the preparation including raw materials, devices and the grinding parameters for different trials. The second part presents a detailed process of the grinding using planetary ball mill. Finally, the extraction method of nanometer zinc oxide powder and the storage of suspension were introduced.

3.1.1 Preparation

The equipments for producing nanometer zinc oxide powder are as follows:

- Fritsch pulverisette-7 planetary ball mill, with a 80 ml grinding jar and 2 mm zirconium oxide grinding balls
- Weighing bowls
- Instruments analytical balance
- 150 millilitres (ml) beaker
- Measuring cylinder
- Metallic table spoon, plastic spoon
- VWR ultrasonic cleaner

The materials used for grinding are:

- Bulk ZnO from Anachemia with the average powder size 500 nm.
- Isopropyl alcohol (IPA)
- Ethylene glycol (EG)
- deionized water (DI Water)

There are five trials we grinded for photodegradation experiments. The parameters for grinding shows below in Table 3.1

Table 3.1 Measurements and ball milling settings used for this project.

Trial name	ZnO-200a	ZnO-400a	ZnO-600a	ZnO-800a	ZnO-1000a
Solvent and Volume (mL)	EG 10 mL	EG 10 mL	EG 10 mL	EG 10 mL	EG 10 mL
Speed (rpm)	200	400	600	800	1000
Grinding beads	100g 2mm	100g 2mm	100g 2mm	100g 2mm	100g 2mm
Grinding time(min)	10	10	10	10	10
Cycles on and off	5 mins on 5mins off	5 mins on 5mins off	5 mins on 10mins off	5 mins on 15mins off	1 mins on 10mins off
ZnO powder (mL)	15	15	15	15	15

3.1.2 Processing

Taking the trial ZnO-600a as an example, I'm going to describe the details of grinding.

Grinding begins with preparation and measurement of grinding powder, solvent, and beads.

a. Powder measurement: I took out the measuring cylinder, rinsed it with IPA and then blew it dry with nitrogen. I used a plastic spoon to remove the powder zinc oxide from the jar and poured it into the measuring cylinder until it read 15 mL. Next I poured 10ml of the powder from the measuring cylinder into the weighing bowl and got the weight of the powder: 10.23g

b. Solvent measurement: The solvent used for trial ZnO-600a is Ethylene glycol (EG). I took another measuring cylinder, rinsed it with IPA and dried it with nitrogen, then poured 10mL EG into the cylinder.

c. Beads measurement: The grinding beads used in trial ZnO-600a were ZrO2 with a diameter of 2 mm and the total weight was 100.8 g measured by the weighing machine. By calculation, the mass ratio of ZrO2 to ZnO powder was 9.85:1, which helped to obtain good grinding since there is more available mass to strike the powder material according to some literatures

After prepared all materials, the next step is to load them into the grinding bowl: I put the measured ZnO powder into the grinding jar with the grinding balls already in it, and then poured the 10 mL EG into the jar. After that, I placed the rubber O-ring on the top lip to ensure an airtight seal, making sure that the notch is near the locking hook. Then I made the two clamps tightly secured and the locking hooks engaged exactly in the middle of the notch. After that, I used parafilm to seal around and inserted the grinding bowl in the grinding machine.

The next thing need to be considered is mass balance. Since the operation speed is relatively high, the planetary ball mill is sensitive to imbalance during operation. To keep this imbalance as small as possible, the mass of all rotations in the system must be

as well balanced as possible, meaning that both grinding stations must always use the same weight. In this project, only one bowl was used for grinding the nanoparticles, so balancing with counterweights was necessary. I measured the total weight of 1.09 kg before inserting the sealed grinding bowl into the machine. Then tried to make the counterweight as heavy as the grinding bowl, which is 1.1 kg here. Finally, I put both the grinding jar and counter weight in the grinding machine.

After all the preparation work, I did the setting of the planet ball mill, using the touch screen to set the total grinding time to 10 minutes and the rotation speed to 600 rpm. The 10-minute grinding time was divided into 2 cycles, with each cycle ‘on’ for 5 minutes and ‘off’ for 10 minutes. During each grinding ‘off’ time, I took the grinding jar out and checked the leakage, pressure and heat. For all the cycles, no leaking was seen outside. At the ‘off’ time of the first cycle, a little pressure released when I loosed the valve on the lid of the bowl. Also, the jar turned really hot so it was necessary to leave the whole jar in the fume hood for some time until it back to room temperature. After 10 minutes, I sealed the grinding bowl again and put it back to the milling machine.

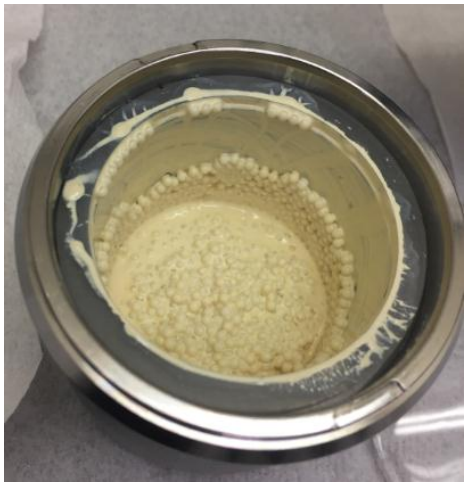

Figure 3.1 ZnO after 10 minutes grinding in the grinding bowl

After grinding for 10 minutes, I took the grinding bowl to the fume hood and waited for it to cool down to room temperature. After turning the press-on valve on lid to

release the pressure, I turned the handle to open the lid. Sometimes the lid can be sticking on the flat seal, so I applied a screwdriver to the actuating pin to remove the lid from the flat seal. Figure 3.1 shows the ZnO with solvent and beads in grinding bowl after 10 minutes grinding.

3.1.3 Extraction

After grinding, it can be seen from figure 3.1 that ZnO nanoparticles were mixed with grinding solvent and beads, and extraction is a necessary step to separate them. I installed the adapter with a stainless steel strainer and sealed tightly against the grinding bowl, pulled tight like a lid, then screwed on the funnel lid for holding the syringe on the adapter, as shown in figure 3.2.

Figure 3.2 Set up for extraction

I carried out 7 times extractions for trial ZnO-600a, and filled the syringe with 10ml solvent (EG) for each extraction. For each time, I injected the 10 mL solvent in the syringe into the bowl, took the whole sealed grinding bowl upside down and shook the bowl for a minute. Then I extracted the suspension into syringe and poured into clean glass vials. Repeated the procedure for seven times and I got ZnO nanoparticles

suspension in glass vials shown below (See Fig. 3.3)

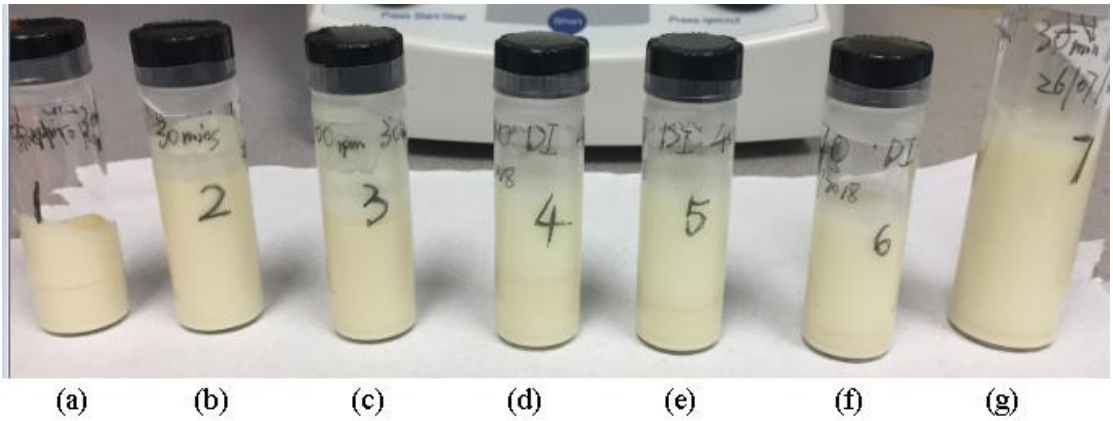

Figure 3.3 Grinded ZnO nanoparticle suspension in glass vials with (a) 1st extraction, (b) 2nd extraction, (c) 3rd extraction, (d) 4th extraction, (e) 5th extraction, (f) 6th extraction, (g) 7th extraction

The catalysts got from planetary ball milling are ZnO-200a, ZnO-400a, ZnO-600a, ZnO-800a, ZnO-1000a. These catalysts are grinded from same pristine ZnO using same solvent for same time. The only different was the grinding speed, which shows in their names. The particle sizes of different ZnO powders are shown in figure 3.4. As can be seen from the figure below, the particle size decreases with the increase of grinding speed. From optical/ AFM analysis, the starting size of pristine bulk is around 500 nm. ZnO-200a is 80% of bulk size, which is 400 nm. For ZnO-600a, 800-a, 1000a, the particle size are around 150nm, 170nm and 100 nm separately. However, these sizes are not a precise values for each and every particle but an estimate average since there is a large distribution.

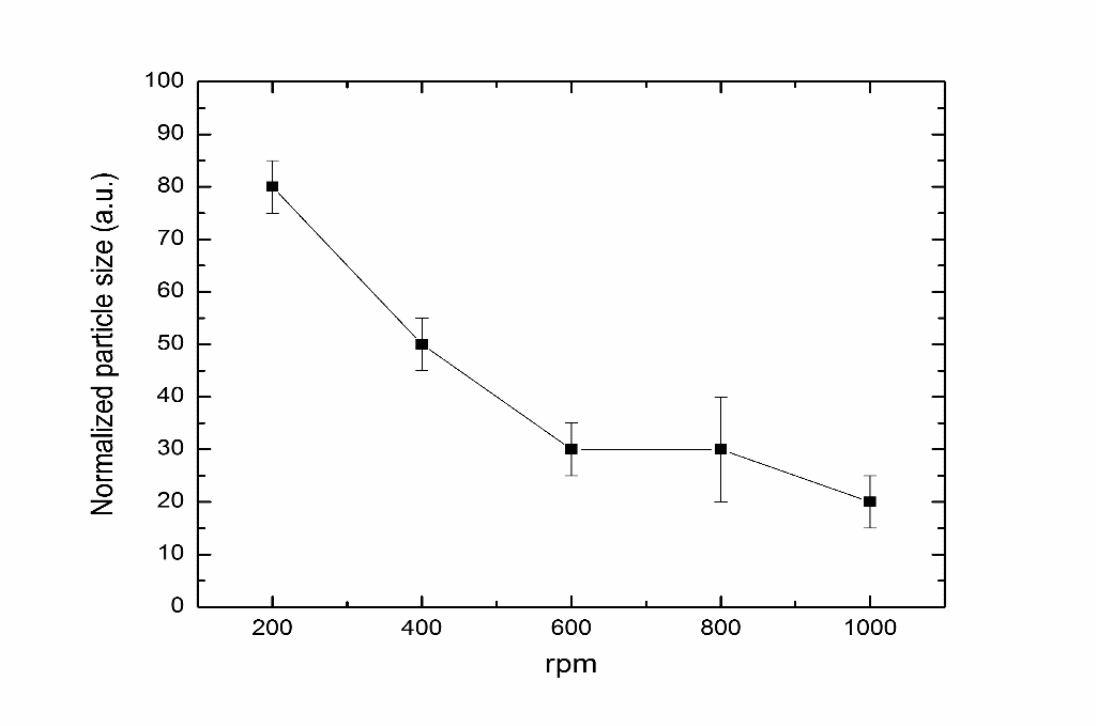

Figure 3.4 Normalized particle size vs. grinding speed

For each dye degradation experiments, the ZnO powders with different particle size were used at the same loading. The volume and initial concentration of BPB dye were same for all experiments. Following the same experiment procedure and sampling method, I can get the degradation result of each experiment. By comparing the result of degradation of BPB dye, I can compare the catalytic ability of ZnO powders with different particle size and discuss how the particle size affect the efficiency of photodegradation.

3.2 Dye degradation experiment set up

3.2.1 Apparatus

The photocatalytic chamber used in this project was designed and constructed in the Nanoscale Research Laboratory at the Department of Engineering in University of Victoria. (See Fig. 3.5) The chamber was illuminated by a 150-watt halogen lamp. Reagents was placed in 8 dram vial reaction vessel designed for photocatalytic reactions at a fixed distance (10cm) from the light source. A plano-convex lens was used in

between light source and reaction vessel to focus light. During reaction, I put a small magnetic stirrer bar in the reaction vessel, and placed the vessel on the magnetic plate.

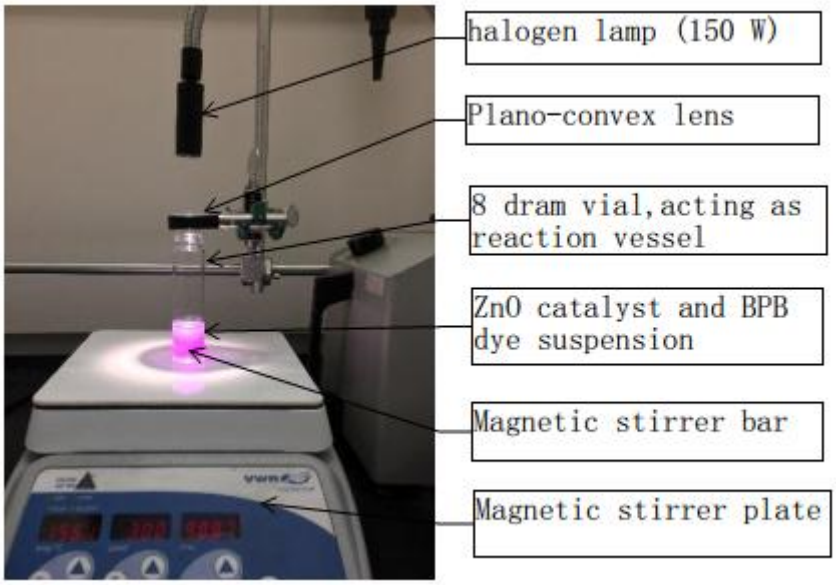

Figure 3.5 Set up for dye degradation experiment

The chamber consists of:

1. Light source, halogen lamp (150 W) to allow constant irradiation during the reaction
2. Plano-convex lens, converging the light of light source to a spot in the reactor.
3. Magnetic stirrer bar and plate, mixing the suspension to reach adsorption equilibrium.
4. 8 dram vial, acting as reaction vessel to hold the suspensions for dye degradation reactions.
5. Pipette, collecting samples during the reaction.
6. Eppendorf centrifuge 5415d
7. VWR 75D Ultrasonic Cleaner, ultra-sonicating the suspension before the reaction to ensure that the catalyst is well-dispersed

8. Fume hood for the photocatalytic reaction to run with continuous stirring. The lens and reactor's position is fixed, so that the distance between light source and reactor is constant.

3.2.2 Preparation of reaction powders

The photocatalysts for the dye degradation experiments are prepared by ball milling method with details presented in section 3.1. The ZnO nanoparticles are stored in glass vials with grinding solvent. (For example figure 3.3). However, the dye degradation experiments require the catalysts in the form of powders. So this section presents the procedure for preparing reaction powders.

First of all, I took the glass vial containing the original suspension and sonicated 20 minutes, then extracted suspension with pipette putting 3 mL of the well dispersed suspension into epi-tubes. After I got the epi-tube with ZnO nanoparticles suspension, I centrifuged it for 10 mins at 10,000rpm and clearly saw the solvent and nanoparticles separated. Then I used pipette to remove supernatant, added DI water to epi-tube and sonicated another 20 minutes to resuspend. I repeated the procedure of resuspending and removing the supernatant three times to ensure that the ZnO nanoparticles were thoroughly cleaned and that there was no grinding solvent attached to them.

After the washing procedure, I got the ZnO nanoparticles deposited on the bottom of epi-tube, and the next step was to dry them to make powders. I put the epi-tubes in oven for several hours at 80 degree, and then took the materials out, crashed them on glass curve, dried in oven again. After the powders were completed dry, stored them in glass vial. The flowchart of washing and drying procedure is shown below.

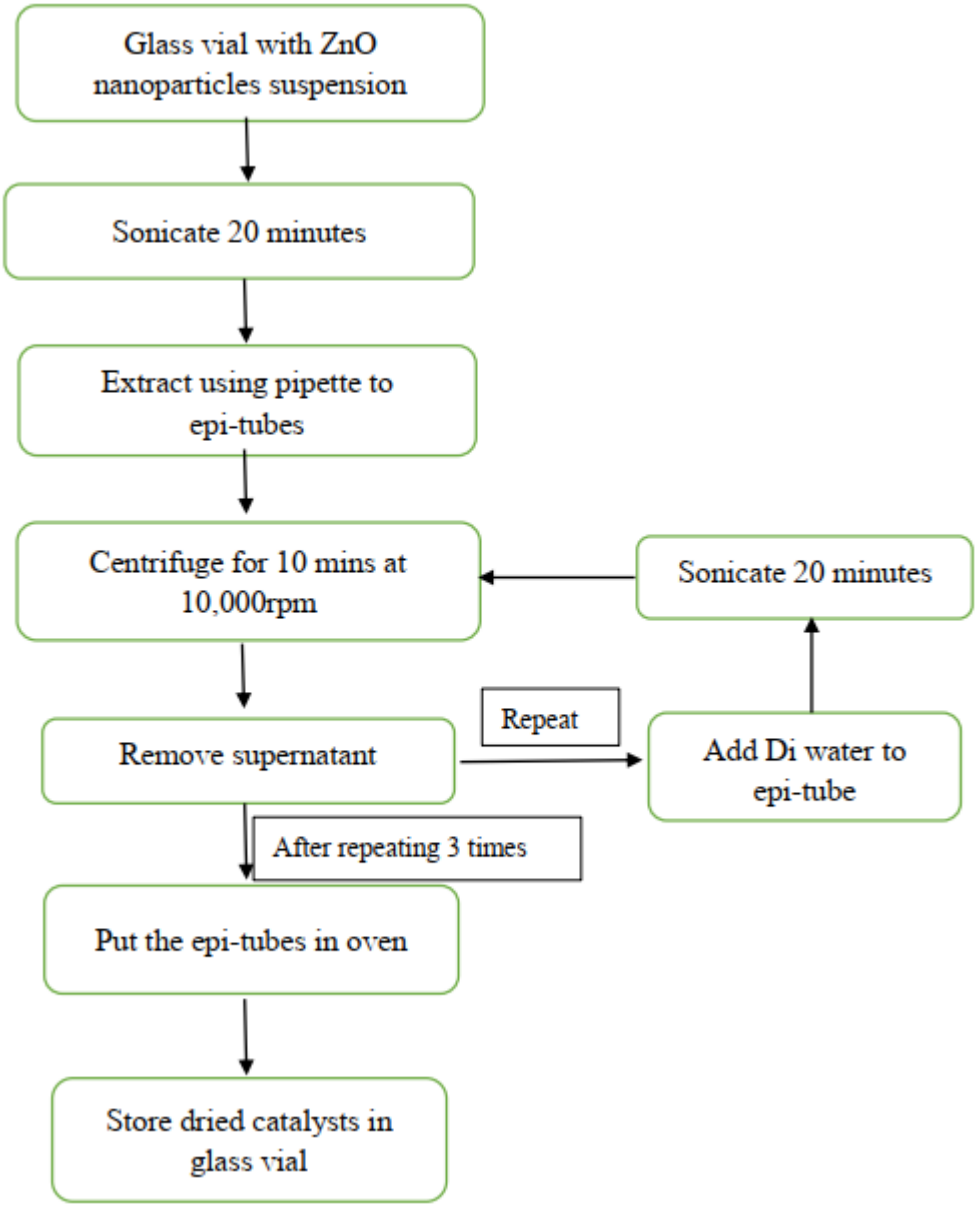

Figure 3.6 Preparation process of reaction powder

3.3 Experiment study

This section describes the experimental steps of dye degradation experiments, including catalyst dispersion, dark reaction and light reaction. Then a controlled experiment was set to study that BPB dye did not degrade in the dark reaction, dark reaction was just help to achieve the adsorption-desorption equilibrium. Next comes the adsorption study, which showed that there was no abvious dye adsorption on the

surface of ZnO. The last part showed that ultrasound would not cause degradation thus affect the performance of photocatalysts in this project.

3.3.1 Dye degradation steps

In all degradation experiments, dye solution was used from stock. To prepare 7ppm BPB solution, I took 1.4 mg of bromophenol blue (BPB) powder and dissolved it in 200 mL of DI water in a beaker, then stirred for half an hour at 500 rpm using magnetic stir. After that, poured the bromophenol blue solution into a glass container and kept in dark place.

1. Catalyst dispersion

The first step of dye degradation experiment is catalyst dispersion. I used pipette to take 10 mL of 7 ppm dye solution from stock into a 8 dram vial. Then I weighted 10mg ZnO catalysts powders using analytical balance and poured it into dye solution. The mixture was first sonicated at powder level 5 for 5 minutes and then put in dark reaction to achieve the adsorption equilibrium of dye molecule on ZnO nanoparticles. During dark reaction, a magnetic stirrer was put into the reaction vessel and stirred at the speed of 300rpm for one hour. The reaction vessel was carefully wrapped by aluminum foil to prevent light from interfering with the dark reaction.

2. Sample method and centrifuge

After dark reaction, dye degradation started under light illumination. During the light reaction, I took samples every hour to see the extent of degradation. Each time, I used pipette to take 1.5 mL of reaction solution and poured into an epi-tube. Then "Eppendorf" centrifuge was used to centrifuge the epi-tube at 10,000 rpm for 10 minutes to separate the catalysts and dye solution, centrifuged for extra 10 mins if the upper solution was not clear. Then another pipette was used to take the supernatant of

the dye solution and stored in a 0.5-dram vial. The following picture shows one example of the supernatant samples of dye degradation experiment using pristine bulk ZnO as catalyst.

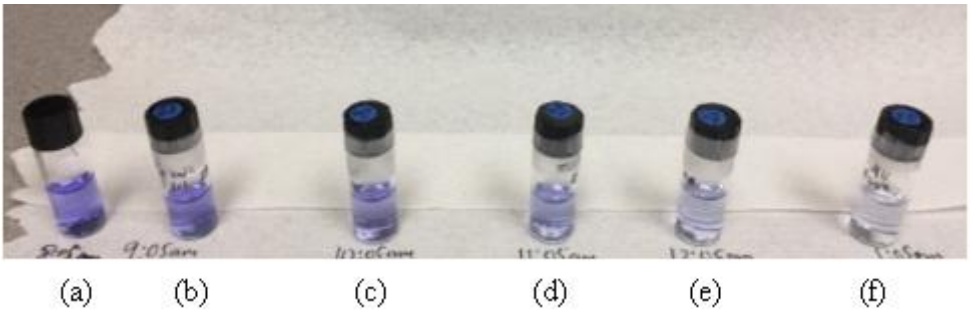

Figure 3.7 Samples of pristine bulk ZnO in dye degradation experiment. (a) Dye solution from stock. Samples taken after (b) dark reaction, (c) 1 hour light reaction. (d) 2 hours light reaction. (e) 3 hours light reaction. (f) 4 hours light reaction.

The first sample (Fig.3.7 (a)) to be taken is the original dye solution from stock, and the color was used as reference. The second sample (Fig.3.7 (b)) was taken after 1 hour of dark reaction, and the color seemed to be the same as the first one. The following four samples (Fig.3.7 (c) (d) (e) (f)) are taken in light reaction every hour, longer time of light reaction leads to better degradation of dye.

3.3.2 Control experiment（Dark reaction）

There are two steps in dye degradation experiment: dark reaction and light reaction. According to the degradation mechanism, the one-hour dark reaction is just to achieve the adsorption-desorption equilibrium, and all the degradation of BPB dyes should occur in the light reaction. In order to check whether this is true for experiments in this project, it is necessary to do a control experiment. For control experiment, everything including set up, initial dye concentration, ZnO loading and so on should be same except for no lighting.

The set up for dark reaction in fume hood include:

1. 8 dram vial, act as reaction vessel, holding the suspensions for dark reactions.
2. Aluminum foil. To wrap the reaction vessel to prevent light exposure and ensure that the whole reaction process is carried out in a dark environment.
3. VWR 75D Ultrasonic Cleaner, ultra-sonicating the suspension before the reaction to ensure that the catalyst is well-dispersed
4. Magnetic stirrer bar and plate, mixing the suspension during dark reaction.
5. Pipette, collecting samples of solution after the reaction.
6. Eppendorf centrifuge 5415d, separating nanoparticles from solution.

The control experiment was conducted with 12ppm BPB dye solution and 7 mg ZnO-400a as photocatalysts. I put a magnetic stir in the reaction vessel and set the stirring speed at 300 rpm. Turned off all light and wrapped the reaction vessel by aluminum foil carefully to prevent room light.

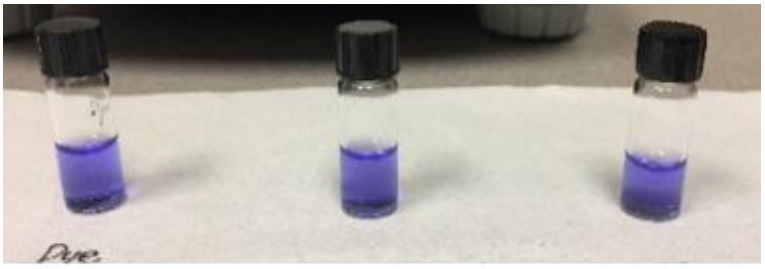

Figure 3.8 Visual appearance of dye solution after centrifuge in control experiment. Same glass vial hold (a) Original 12ppm BPB dye solution, (b) BPB dye after 1 hour dark reaction (c) BPB dye after 19 hours dark reaction

The control experiment was last for 19 hours and the result was shown in figure 3.8. The left vial (Fig.3.8 (a)) held the original dye solution from 12ppm stock. The middle and right vial (Fig.3.8 (b) and (c)) presented the color of BPB dye after 1 hour and 19 hours dark reaction separately. From the visual appearance, no color degradation was observed after 19 hours. The control experiment showed that no degradation occur during dark reaction under the experiment conditions in this project.

3.3.3 Sonication effect

In the catalyst dispersion, one of the steps is to sonicate the dye and catalyst suspension for 5 minutes and stir in the dark for 1 hour to achieve the adsorption/desorption equilibrium. However, ultrasound may cause decolorization of dyes, the mechanism of which was discussed in detail in section 2.3.4. This section is to do experiments to study whether sonication can cause decolorization thus affect the performance of photocatalysts in this project.

The first experiment was to study whether ultrasound would affect BPB dye in the absence of a catalyst. I took the prepared 7ppm dye solution from stock, used pipette to filled 4 small glass vials with 1.5ml each. Then I set the power of the ultrasonic machine to level 5, which is the same as the dye degradation experiment. The first sample was retained as a control group and no ultrasound was performed at all. The second vial was sonicated for 5 minutes, the third for 30 minutes, and the fourth for 60 minutes. I compared the color of four bottles of dye solutions and found that they were identical, proving that the ultrasound did not degrade the BPB dye within 60 minutes.

Next experiment is to check if sonication can help the catalyst degrade the dye. To study that, ZnO-200 nanoparticles were used as catalysts and the initial dye concentration was 7 ppm. I poured 10 mL dye solution into a 8 dram vial (reaction vessel), added 10 mg of catalysts ZnO-200 into it, and sonicated the suspension for 5 minutes. Then I used pipette to take 1.5 mL suspension out as a sample and continued sonicating the 8 dram vial for another 25 minutes. After the total 30 minutes sonication, I took another 1.5 mL suspension as the second sample. With the two samples, I centrifuged them 10 minutes at 10000 rpm, removed the supernatant into small vials and compared the color with the original dye solution. Figure 3.9 shows the color comparison between original dye(a), sonication the suspension 5 minutes(b) and 30 minutes(c).

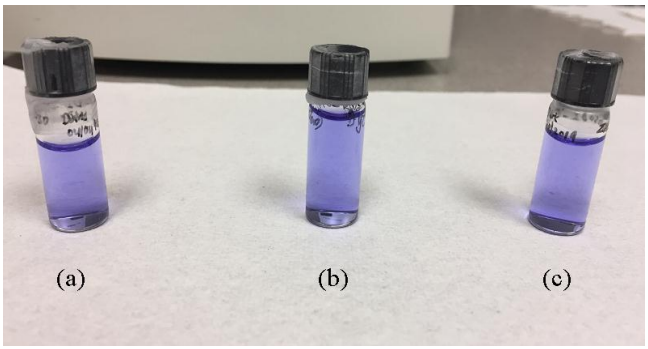

Figure 3.9 Color comparison with (a) Original dye, (b) suspension sonicated 5 minutes (b) and 30 minutes(c)

As can be seen from figure 3.9, the color of the three vials are identical, which proves that the BPB dye will not be degraded during the ultrasonic process. According to section 2.1.2, the basic structure of BPB is that three benzene rings are connected to the same carbon atom, which makes the chemical relatively stable and difficult to degrade by ultrasonic alone. In addition, the ultrasonic time of dye degradation experiment in this project was only 5 minutes, during which no degradation occurred. Sonication was used to only mix the suspension well and help achieve the adsorption-desorption balance.

3.4 Dye degradation with ZnO nanoparticles

3.4.1 ZnO nanoparticles with different particle sizes

The catalysts discussed in this section are ZnO-200a, ZnO-400a, ZnO-600a, ZnO-800a and ZnO-1000a. These catalysts were grinded from same pristine ZnO using same solvent for same time with only difference in grinding speed, which is shown in their names. The faster the sample was grinded, the smaller particles size and the larger surface area.

In each experiment, the ZnO nanoparticles were used at the same loading, the volume and initial concentration of BPB dye were also same. So each time, I poured 10 mL of

the 7 ppm BPB solution into the reaction vessel (8 dram vial), loaded 10 mg of ZnO catalysts into it, followed the same experiment procedure of catalyst dispersion and 4 hours light reaction, and the results of degradation using different ZnO catalysts were shown in figure 3.10.

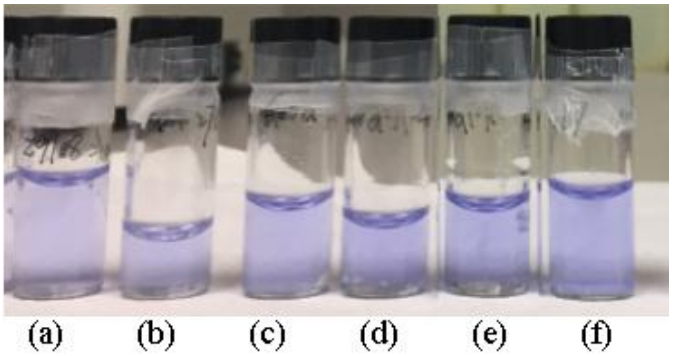

Figure 3.10 Degradation results for different ZnO catalysts. (a) pristine bulk ZnO, (b) ZnO-200a, (c) ZnO-400a, (d) ZnO-600a, (e) ZnO-800a and (f) ZnO-1000a.

The color of the degradation result can indicate the catalytic ability of the nanoparticles. The BPB dye is dark blue, and the lighter the color is after degradation, the lower the concentration of BPB dye, which means the better catalytic performance of the nanoparticles. After the experiments using different ZnO nanoparticles, we sorted the bottles by the color of the solution inside, as shown in figure 3.10. For now we observe with bare eyes, in the future, we may use ultraviolet–visible spectroscopy (UV–Vis) to measure the concentration of BPB to get better comparison. In figure 3.10, from bottle (a) to (f), the color turns darker, that means the decreasing photocatalytic ability of the corresponding nanoparticles. Bottle (a) shows the lightest blue color which degraded by pristine bulk ZnO, so it can be inferred that pristine bulk ZnO has the best catalytic ability.

By comparing the degradation result of catalysts ZnO-600a and ZnO-400a, it was found that ZnO-600a had better catalytic performance. The particle size of ZnO-600a was around 150 nm, much smaller than ZnO-400a, which is 250 nm. The better

performance of ZnO-600a may be due to its large surface area, which enabled more dye molecules to adsorb on the catalyst surface, thus improving the photodegradation efficiency. In addition, ZnO-600a may had more dispersed particles per volume in solution, which also contributes to degradation.

It can be seen from the degradation results that the degradation rate of ZnO-400a is faster than that of ZnO-800a and ZnO-1000a, which illustrate that the smaller particles size doesn't necessarily mean higher degradation efficiency. There are many other parameters that may also affect the reaction efficiency, such as crystallinity, particle morphology and so on. Sometimes crystallinity and high surface reactivity are more important for photocatalysts. One of the most important characteristics of active zinc oxide is the abundance of specific sites, which are closely related to the preparation route.

By comparing the degradation result of bulk ZnO powder with grinded ZnO nanoparticles, it can be seen that the degradation rate of pristine bulk powders degrades was faster than all grinded catalysts. The reason for the decline of catalytic performance of zinc oxide after grinding may be the high density bulk defects produced by mechanical ball mill. These bulk defects acted as recombination centers and greatly inhibited the separation of photo-generated charges greatly and thus reduced photocatalytic activity.

The result suggested that the photocatalytic activity of ZnO samples could not be evaluated from the particle size alone, because the bulk defects, active surface area, crystallinity, particle morphology and other factors also play an active role on the photodegradation efficiency.

3.4.2 ZnO nanoparticles from manual grinding

From the previous ball mill samples, we can see that all the ZnO mill samples turned

yellow, although the original bulk ZnO was white. See figure3.1 and 3.3 for example. This color change result was consistent with paper [76]. One of their samples, ZnO(1000) turned yellowish after several hours of grinding and dark yellow after grinding 100 hours.

There are several possible reasons to determine the color change of ZnO powder, and the first thing to be considered is the preparation process. When grinding the ZnO, mechanical and chemical reactions can happen, resulting in many defects including interstitial Zni, oxygen vacancy and so on, which are all related to oxygen.

To investigate whether oxygen plays a role in the grinding process, resulting in the decreasing of the photocatalytic properties of ZnO, I designed experiments to manually grind zinc oxide powder in air and nitrogen environment. I used mortar and pestle which are made in a matching set of ceramic to grind commercial ZnO manually. The mortar is a small bowl and the pestle is a wand with a curve which is perfectly shaped to grind smoothly against the mortar.

Grinding in air

I weighted the ZnO bulk powder 201.2 mg and put into the mortar which is cleaned thoroughly by Isopropyl alcohol (IPA). Then I hold the mortar in place with one hand and the pestle in the other and twisted it against the ingredients in the mortar so that they are ground on the bottom and sides of the mortar. Evenly grind, bash or crush all the powders for 10 minutes, I used the pestle to mix and grind them until they are all reduced to the same consistency.

I clearly saw that the grinded ZnO turned yellowish after 10 minutes grinding. Then I put the freshly ground ZnO into a glass vial with a tight-fitting lid, and used parafilm to seal the lid.

Grinding in N2 environment

Next, I tried to measure the same amount of bulk ZnO powder, put in mortar and grind in N_2 environment for 10 minutes.

xs

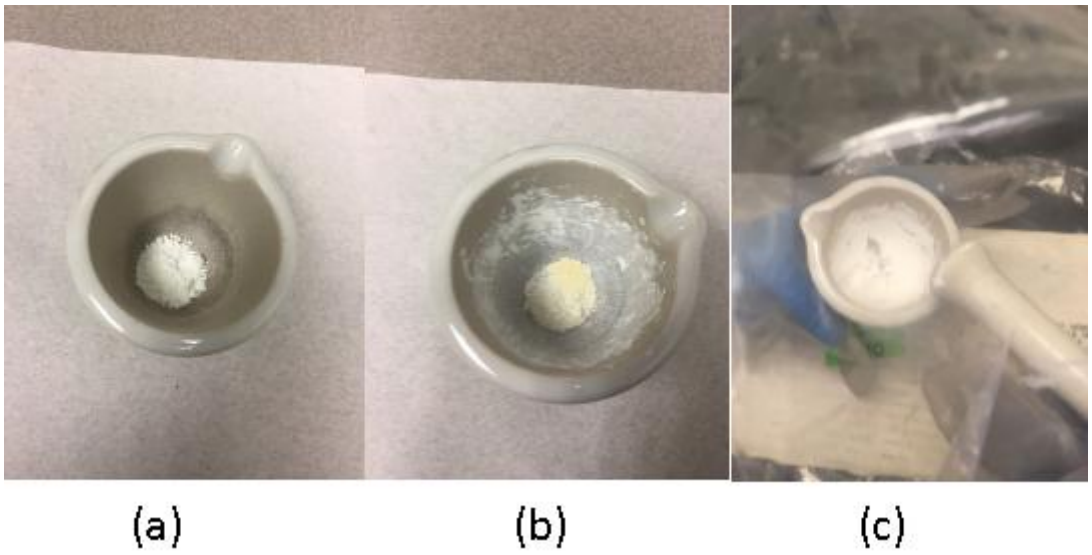

Figure 3.11 ZnO remain white after 10 minutes manual grinding in N2. ZnO powder (a) before grinding (b) after grinding in air (c) after grinding in N2

To generate N_2 environment, I used glove bag called 'hand in bag', a flexible, inflatable, polyethylene chambers with built-in gloves that works in a totally isolated and controlled environment. I stabilized the glove bag in fume hood, placed all necessary equipment inside the glove bag, including the clean mortar and pestle, bulk ZnO powder and so on. Then I connected the glove bang with gas source tightly and secured with tape, turned on nitrogen gas and allowed gas to gently flow out. I did 3 vacuum/inert gas purge cycles to make sure that all work was done in over 99% nitrogen environment.

Then I followed the same procedure of grinding for 10 minutes as I did in the air, and the result is shown in figure 3.11. Different from the yellow powder in the air, the grinded ZnO in N_2 remained white, so we can say that the color change of ZnO during

the grinding is related to oxygen.

After preparing two ZnO catalysts from manual grinding, we got two samples ZnO-O_2 and ZnO-N_2. I used BPB dye to test their dye degradation ability and the result is shown in figure 3.12.

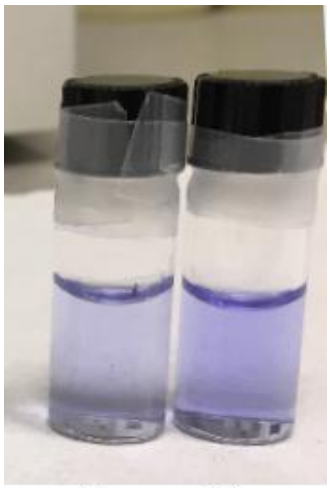

Figure 3.12 Degradation result for manual ZnO catalysts (a) ZnO-N_2 (b) ZnO-O_2

It can be seen that the dye color turned lighter after degraded by catalyst ZnO-N_2, indicating that the degradation capacity of ZnO-N_2 is better than that of ZnO-O_2. By comparing the catalysts ground in different environments, it can be inferred that oxygen was involved in these mechanochemical reactions, causing color changes and defects in ZnO, and reducing the photocatalytic capacity of ZnO.

Chapter 4 Discussion and Future work

4.1 Discussion

In this project, planetary ball milling method was used to synthesis nanomaterial. There are many advantages of ball mill, for example the ball milling machine is reliable, can provide good operating conditions, crushing in a closed jar and no dust flying. In addition, the planetary ball mill can be used for both dry and wet grinding, intermittent or continuous operation. When crushing explosives, inert gas can be used instead of air for crushing.

However, there are also disadvantages of ball grinding that needed consideration. First of all, it's a top-down method and it's hard to get accurate size of nanoparticles. Taking the grinded material like ZnO-200a, 400a, 600a, 800a and1000a as example, we can only estimate average size due to the large distribution, which limited us to accurately calculate the different relations of material property with particle size.

Another concern we have for using ball mill is contamination. When the dye degradation experiment was carried out with the grinded ZnO, the result can be affect by the contamination of grinding ball and solvent nanoparticles. The grinding ball we used in this project is made of ZrO2. With strong friction and crush, there was high chance that ZrO2 nanoparticles may blend in grinding material. Also, all the grinding trials in this project were wet grinding with solvent like IPA or EG. Although there was a procedure to 'wash' the powders, solvent particles can still stick around reaction nanoparticles.

In section 3.3, I used ZnO nanoparticles with different particle sizes prepared by planetary ball mill, followed the procedure to do dye degradation experiment, tried to study the relationship between ZnO material properties and photocatalytic activity. In

theory, if all other properties of ZnO are same, the photocatalytic ability should increase with the decrease of particle size. However, according to our result, ZnO-1000a with the smallest particle size and the largest surface area didn't show the best catalytic ability, indicating that photocatalytic activity of a ZnO samples could be evaluated only by particle size. Factors such as volume defect, active surface area, crystallinity and particle morphology also play an active role in photodegradation efficiency. These properties are interrelated and must be considered as a whole.

4.2 Future work

Semiconductor photocatalytic technology as an effective environmental pollutant treatment technology has broad application prospects. Research on semiconductor characteristic and modification are also a hotspot in the field of photocatalysis. Zinc oxide has attracted more and more attention in recent years because of its characteristics. We successfully prepared ZnO nanoparticles catalysts using ball milling method and designed experiments to test the dye degradation ability. However, there is still much to be done.

4.2.1 Characterization and quantitative analysis

In the future, we need to characterize our synthesized nanoparticles, including lattices, morphologies, and defects. In addition, it is better to conduct quantitative analysis on the degradation of dyes, measure the concentration of dye solution in the experimental process, and calculate the degradation efficiency.

Catalyst characterization

In order to have a better understanding of structural properties and crystallite size of the ZnO trial we grinded, it's better to do X-ray diffraction (XRD). X-ray diffraction refers to the analysis of the X-ray diffraction pattern of a material to obtain information such as the composition of the material and the structure or morphology of the atoms

or molecules inside the material.

The average crystallite size (D) can be calculated using Scherrer formula (Eq. 4.1). In the equation, λ is the wavelength of the incident X-ray beam, β is the full width at half maximum (FWHM) and θ is the Bragg diffraction angle.

$$D = \frac{0.9\,\lambda}{\beta\,cos\theta} \qquad (4.1)$$

Raman spectra is needed for further understanding of the crystal quality. Planetary ball milling can affect the crystal quality of the grinded ZnO. According to the degradation results, although the particle size of ZnO-1000a is the smallest, its catalytic performance is not the best. We speculate that the crystallinity and morphology of ZnO will affect its photocatalytic performance. In order tocompare the consequent changes in the morphology of different ZnO trials after grinding, Scanning Electron Microscope (SEM) and Field Emission Scanning Electron Microscope (FESEM) studies can be carried out.

To analysis the optical properties of the ZnO trials, we can use record the room temperature photoluminescence spectrum (PL). Zinc oxide usually has two emission peaks, a strong emission peak in the near ultraviolet region and a relatively weak and wide emission peak in the visible region.[77], There are relations between emission and particle defects. The NBE emission is originate from the direct recombination of free electrons and holes. Some visible emissions are originate from the radiative recombination from different defect states including oxygen vacancies (Vo), zinc vacancies (VZn), zinc interstitials (Zni), oxygen interstitials (Oi)[78]. Using photoluminescence spectrum can helps to determine the ZnO defects on grinded trials.

To better evaluate the type of defect, positron annihilation spectroscopy (PAS) can be used. This is a non-destructive and sensitive way to measure the vacancies and open

volume defects in solids. Due to the decrease of electron density and the change of electron momentum distribution, the characteristics of electron momentum and positron annihilation lifetime are modulated by vacancy defects. [79]Depending on the annihilation time and the momentum distribution of the electrons, the type of defects can be evaluated. By understating the exact type of defects on ZnO trials, we can better explain how these defects can affect the catalytic ability.

Degradation analysis

In order to measure the degradation rate, it is necessary to monitor the changes of the maximum molecular absorption of BPB dye throughout the experiment. An aliquot (1.5 mL) of the solution from the mixture was taken every hour and then centrifuged. Ultraviolet–visible spectroscopy (UV-Vis) can be used to evaluate the photocatalytic degradation by recording the maximum absorption spectra of the BPB dye solution. The photodegradation efficiency (η) of BPB can be calculated as follows[33]:

$$\eta = \frac{C_0 - C_t}{C_0} * 100 \qquad (4.2)$$

C0 is the initial concentration of BPB and Ct is the concentration of BPB after‘t’ min reaction time. The degradation efficiency in this report is calculated at a time period of 240 min. In the presence of ZnO, the absorbance peak of BPB decreases with the reaction time denoting the efficient photocatalytic activity of ZnO.

To study control experiment, which is the adsorption property of the ZnO, we can follow the same experimental procedure，repeat the experiment in dark for 240 min at room temperature and check the concentration of BPB all through the experiment.

4.2.2 Doping material

Improving the catalytic performance of photocatalytic materials has always been the

focus of research. In this project, we have studied the catalytic performance of ZnO, and there are still a lot we can try to improve the dye degradation rate of ZnO. Due to the large band gap of zinc oxide, light absorption can only be carried out near the ultraviolet region, and the visible light absorption is relatively low. Moreover, photogenerated carriers of ZnO are easy to recombine, and the quantum production is very low. Improving the photocatalytic activity and efficiency as well as increasing the spectral response range of zinc oxide are major difficulties in photocatalytic technology.

The doping materials we can try are Ag, Se, graphene and so on. One of the reasons that doping can increase the catalytic ability of ZnO is that doping particles can act as shallow potential traps to inhibit the recombination of photogenerated electrons and holes. Another reason is that doping metals can change the band structure of semiconductors, helping to absorb more low-energy photons and increasing the utilization of light source. Doping can form doping level, which is located between CB and VB[80], excites photons with longer wavelength and lower energy, shows the red shift of absorption spectrum, and improves the utilization rate of photons.

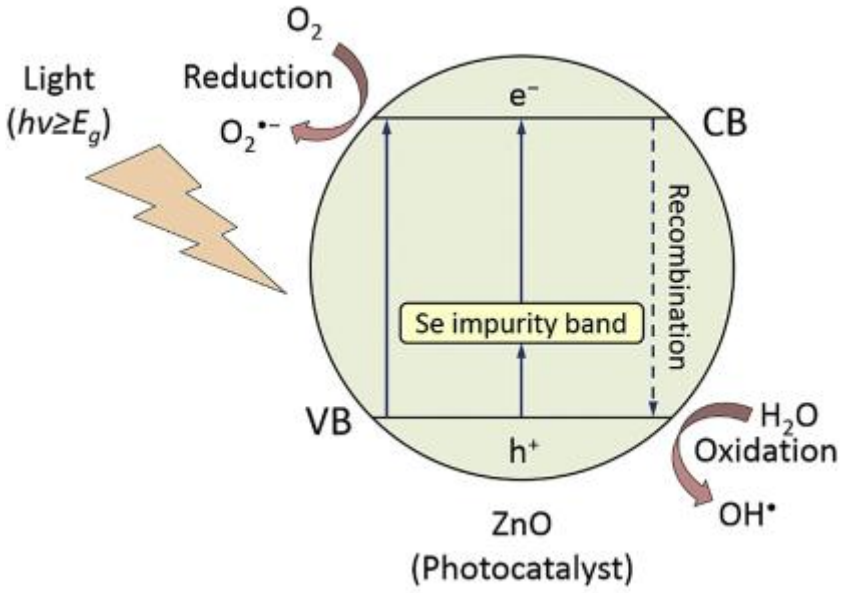

Figure 4.1 Photocatalytic mechanism of Se-doped ZnO nanoplates [81]

Choi, Young In, et al.[61]explained that when the Ag doped semiconductor is under illumination, the electronics generate in conduction band can migrate to the Ag particles. So, Ag particles can be regarded as a temporary storage of photogenerated electronics, which can effectively prevent the recombination of electrons and holes, so as to improve the photocatalytic activity. In the future, ZnO nanoparticles can be doped with silver by the method of planetary ball milling, and the band gap of ZnO can be engineered by ball-milling and Ag hybridization. Chen, Yuanlu, et al.[81]synthesized Se-doped ZnO nanoplates using high-energy planetary ball mill 8000M-230 (SPEX Sample Prep, USA), which showed better photocatalytic activity under visible-light illumination than undoped ZnO. The photocatalytic mechanism of Se-doped ZnO nanoplates is shown in figure 4.1, Se impurity band existed between the band-gap of Se-doped ZnO, captured the photogenerated holes, which reduce the recombination of free electrons and holes and improved the photocatalytic performance.

Lonkar, Sunil P., Vishnu V. Pillai, and Saeed M. Alhassan [82]synthesised the ZnS-ZnO/graphene heterostructured nano-photocatalysts using ball milling followed and thermal annealing. The schematic diagram of charge separation and photogenerated carrier transfer is shown in the following figure, which explains why the presence of graphene plays an important role in enhancing the visible photocatalytic activity of ZnS-ZnO heterostructure. First, through the percolation mechanism, effective electron transfer of ZnS-ZnO to the graphene reservoir can reduce the rate of electron-hole pair recombination. Second, under visible light irradiation, graphene generates photoexcited electrons, which are then transferred to CB of ZnS-ZnO, thereby transforming wide-band gap ZnS-ZnO into visible photocatalyst. What is more, because of the special electron conductivity, the layered graphene network can facilitate the rapid migration of reactive carriers, which may lead to charge separation.

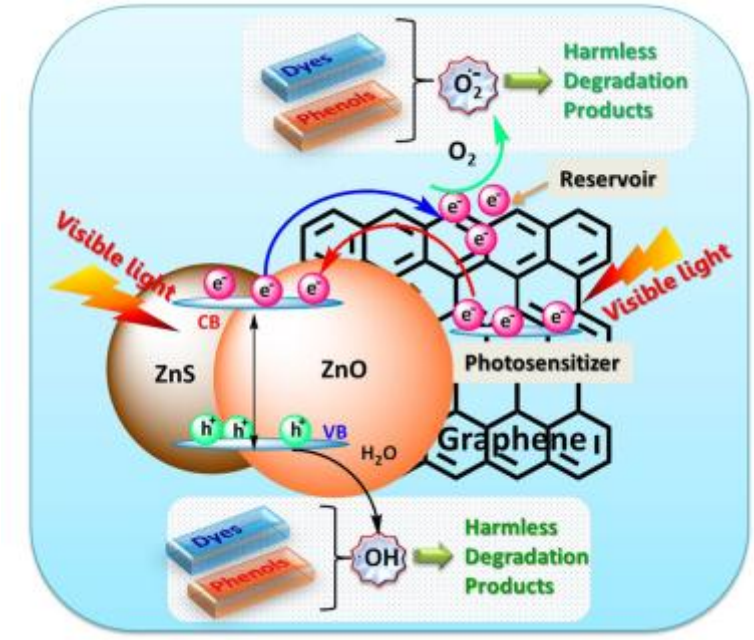

Figure 4.2 Schematic illustration of the charge separation and the transfer of photo-induced charge carriers in ZnS-ZnO/graphene heterostructured nano-photocatalysts for dye degradation under visible light irradiation [82]

However, doping and modification methods may also cause changes in surface properties, crystal structure and other characteristics of zinc oxide. In future experiments, we need to understand that whether doping will lead to better results in dye degradation experiments also depends on the parameters and process of doping. For example, if the doping ratio of Ag/graphene to ZnO is too large, then too many traps will easily deactivate the excited carrier during the transfer. In addition, although Ag/graphene can cause surface defects that increase the efficiency of free radical formation, it can also cause bulk defects, which are recombination centers that decrease the catalytic performance.

4.2.3 Other particle types

In addition to zinc oxide, we can also try other types of nanoparticles as photocatalysts, such as Titanium disilicide, Silicon and carbon based materials.

Titanium disilicide (TiSi2)

TiSi2 is a non-toxic gray intermetallic compound with better electrical conductivity and thermodynamic stability than other silica-titanium compounds. There are two different crystalline phases. One is the low temperature metastable phase C49 structure, the other is the high temperature stable phase C54 structure. [83]C54 has a better conductivity, and the resistivity is 13-20μΩ·cm. C54 has high melting point (1813K), good thermal stability, and has been widely used in microelectronic integrated circuits.

The crystal structure of TiSi2 is shown in figure 4.3. The left one presents C54 structure, which is a Ti16Si32 cluster. The right one presents C49 with two Si layer of Ti20Si40 cluster.

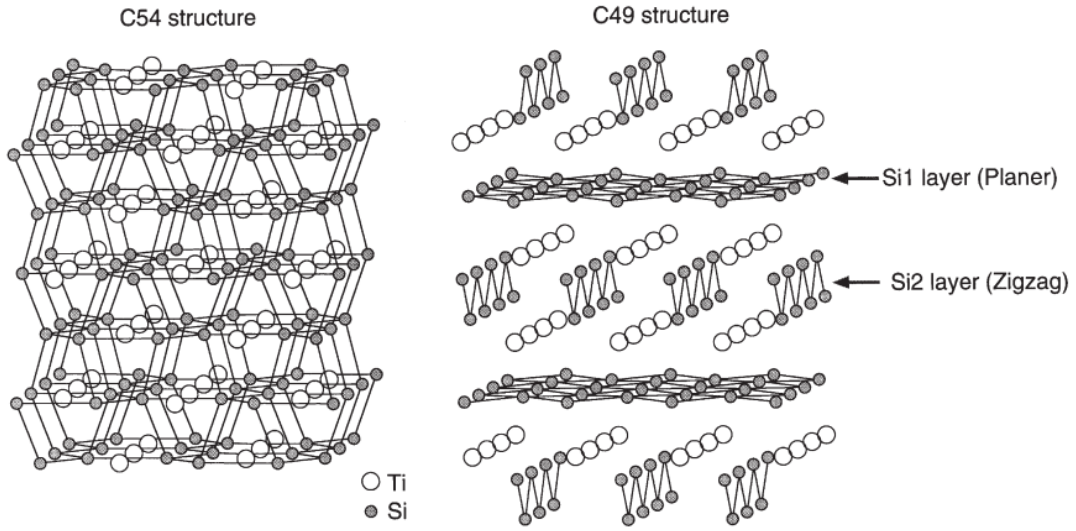

Figure 4.3 Crystal structures of C54 and C49 TiSi2 [83]

In light absorption characteristics, TiSi2 has a band-gap range from 3.4 eV (ca. 360 nm) to 1.5 eV (ca. 800 nm), which is ideal for solar applications. It reported [84]to be used in photocatalytic water splitting to generate hydrogen and oxygen due to its well light absorption performance. Liu, Jianjun, et al.[85]prepared Ti–Si powder mixtures using a planetary ball-miller of Fritsch P7 made in Germany in nitrogen atmosphere and evaluated the photocatalytic activity of splitting water into hydrogen under visible light. The result showed that TiSi2 can be a good photocatalyst. So we may try to use

TiSi2 to degrade the dye and test its photocatalytic degradation ability.

Silicon (Si)

Silicon is the eighth most abundant element in the universe, accounting for 27.71% of the earth's crust, which is the second most abundant element in the earth's crust after oxygen.[86].In nature, however, it is hard to find silicon in its free state. With the development of industry, the demand of semiconductor industry increases, and the purification technology of silicon material has made great progress. Now, silicon is a mature semiconductor material with large annual production and gradually reduced cost.

Common silicon exists in amorphous and crystalline states. Among them, crystalline silicon is silver-gray with metallic luster, hard and brittle, with diamond structure. At room temperature, silicon has a band gap of 1.12eV, is opaque to visible light, and can absorb ultraviolet and visible bands and a small amount of infrared light. At room temperature, silicon intrinsic carrier density is 1.5*10^10 per cubic centimeter, its corresponding resistance is 2.3 * 10^5 Ω · cm. Melting point is about 1690 K. Electron mobility is about 1350cm^2/V s and hole mobility is about 480 cm^2/V s. [86]

Si quantum dots can also be used as photocatalyst attributable to their adjustable band gap and good photoconductivity properties. Kang, Zhenhui, et al [87]proved that 1-2 nm Si quantum dots can indeed be used as good photocatalysts for CO2 reduction and dye (methyl red) degradation. While 3-4 nm Si quantum dots are only effective photocatalysts for selective oxidation of benzene, not able to induce degradation of methyl red nor photochemical reduction of CO2 due to the less energy of electron-hole pairs. The details are shown in figure 4.4.

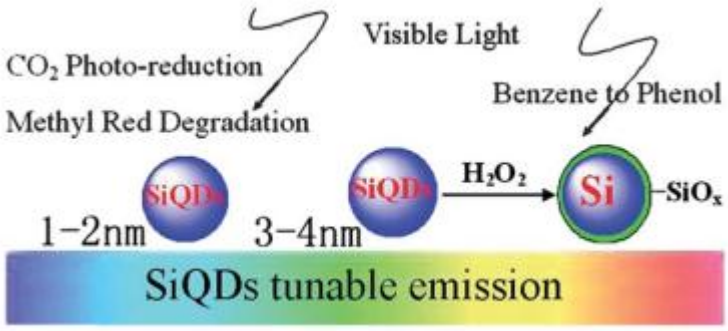

Figure 4.4 Different Diameters Silicon Quantum Dots（SiQDs） for Different Reactions [87]

Planetary ball milling method can be used to synthesis silicon nanoparticles (SiNPs) Kuang, Li, Brian S. Mitchell, and Mark J. Fink.[88] prepared silicon nanoparticles from silicon wafers using a 65-ml hardened steel ball milling vial with two hardened steel milling balls (1.2 cm in diameter, 8.1 g each) in a nitrogen-filled glove box. More novel catalysts can be designed and synthesized by doping Si with other materials including TiO2, ZnO, graphene and so on.

Carbon-based materials.

Ball milling can be used to prepare different kinds of carbon based materials. For example, Pan, Hualong, et al [89] used ball milling to modified single-walled carbon nanotubes (SWNTs) by a mixture of SWNTs and KOH. Wang, Zhengshang, et al.[90] systhesized graphene oxide (GO) by grinding graphene sheets and ZrO2 at 300 rpm for 50 hours. Nitrogen-doped GO (N-G) catalyst[91] and Multiwalled CNTs (MWCNTs) [92]can also be synthesis by ball milling method. Figure 4.5 illustrates a schematic of mechanochemical reaction between graphite and C60 in a sealed ball-mill crusher.

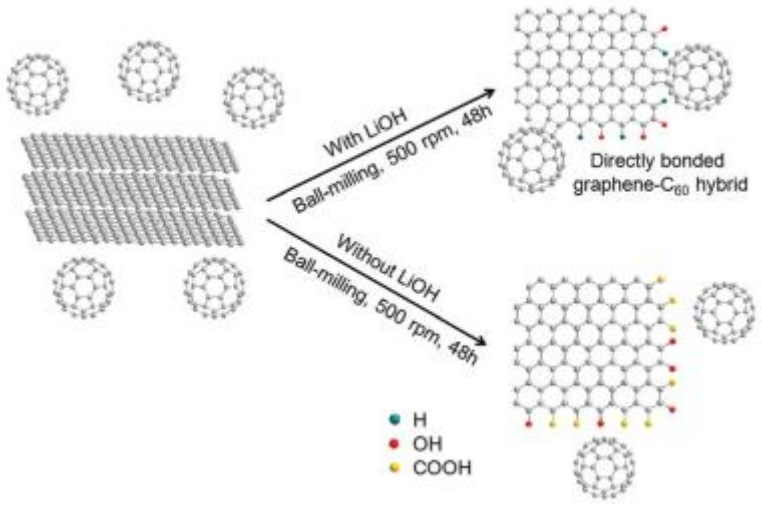

Figure 4.5 Schematic illustration of the mechanochemical reaction between graphite and C60 in a sealed ball-mill crusher. The synthesis routes with LiOH affording the directly bonded graphene–C60 hybrid or without LiOH leading to the formation of oxygenated graphene nanoplatelets and unreacted C60 are both shown [93]

The prepared ball milling carbon nanomaterials (BM-CNMs) can be used in contaminants remediation. Fu, Chenxi, et al. [94] used ball milling to product few layered and large-scale graphene sheets and successfully degrade 99% of the cationic dye, Methylene blue (MB) within 700 min at room temperature. He, Guangyu, et al.[95]prepared CoFe2O4−Reduced Graphene Oxide Heterojunctions using ball milling method and proved its photocatalytic ability on degradation of methylene blue, rhodamine B and methyl orange under visible-light irradiation. Santos, Diogo FM, et al.[96]treated Multi-walled carbon nanotubes (MWCNTs) by ball milling under nitrogen atmosphere and proved the N-doped MWCNTs to be good photocatalyst for the degradation of phenol in aqueous solution.

4.2.4 Environmental application

From the perspective of environmental application, catalyst dispersion and solid-liquid separation recycling issues should be considered. The catalysts used in this project are all in powder form, so it is necessary to study the improvement of photocatalyst fixation in the actual wastewater treatment, so as to meet the requirements of industrialization.

Also, more consideration should be given to the application of natural sunlight. Although the prepared catalysts can realize photocatalytic degradation of organic dye under visible light, many factors have not been considered in the experimental process. For example, the effect of light intensity on degradation efficiency, the duration of sunlight and the problem of cost.

From the perspective of other applications, photocatalyst ZnO can not only be used to degrade dyes, but also can help produce hydrogen, solving the problem of energy shortage. Since the discovery that hydrogen and oxygen can be produced by photodissociation of water with TiO2 semiconductor electrode[6], the research on the catalytic performance of photocatalytic materials has attracted much attention. The research on catalytic properties of zinc oxide and the methods to improve the catalytic properties of zinc oxide can also be used in hydrogen production.

4.3 Summary and Conclusion

The subject of photocatalysis is a new interdisciplinary subject of catalytic chemistry, semiconductor physics, photoelectric chemistry, material science and environmental science. The breakthrough in the application of photocatalyst will solve environmental and energy problems facing mankind in the 21st century. Photocatalysis has become an ideal technology for clean energy production and environmental pollution control due to its unique performance of deep reaction at room temperature and direct use of sunlight as a light source to drive the reaction. In this project, the photocatalyst was prepared by ball milling method and used for degradation of organic dyes.

Chapter 1 presented a comprehensive literature review on textile dye, nanomaterial, semiconductor-based photocatalysts and planetary ball milling. The chapter began with an introduction to the classification of dyes and the general chemical structures that produce specific dye colors, and how advanced oxidation processes (AOP) degrade

dyes. Then the basic principle of semiconductor photocatalysis was introduced. Using photocatalyst to generate photocarriers to degrade dye belongs to advanced oxidation method. After that, the properties and applications of nanomaterial were reviewed, and the advantage of preparing nanosized photocatalysts by planetary ball milling were discussed.

Chapter 2 was focused on the photodegradation reaction mechanism. The catalytic properties of zinc oxide were introduced and the degradation mechanism of bromophenol blue was proposed. Then I proposed a photodegradation reaction mechanism, which include electron-hole pair generation, charge-carriers reaction and degradation of dye compounds. The the parameters affecting photodegradation including surface area, volume defect, surface defect and ultrasonic effect were discussed.

Chapter 3 introduced the synthesis procedure of ZnO nanoparticles including preparation, processing as well as extraction, and the procedure to conduct dye degradation experiments. The catalysts used in this project were prepared by planetary grinding method, and then the reaction powder was generated according to the "washing" procedure. BPB dye was used as an organic pollutant with initial concentration of 7 ppm (7mg/L). Photocatalytic dye degradation experiments were carried out in the reaction chamber with halogen lamp (150w) as light source. The catalyst dispersion method was to sonicate the suspension of catalyst and dye for 5 minutes, then stirred in dark for one hour to reach adsorption-desorption equilibrium. The standard reaction period is 5 hours, including 1 hour dark reaction and 4 hours light reaction. However, in some cases, a longer reaction time may be used (for example, control experiment). The sample method was to take 1.5 mL of sample per hour and centrifuged it at 10,000 rpm for 10 minutes, took the supernatant and stored in glass vial and compared the degradation color.

The particle size of catalyst is an important parameter that affects the

photodegradation efficiency. When the ZnO particle size is reduced, the surface area of the ZnO photocatalyst increases and the number of dispersed particles per volume in the solution increases, resulting in an increase in the photoreaction. The results in this project showed that ZnO-600a had better degradation performance than ZnO-400a, which was consistent with the theoretical analysis. However, the result also showed that the pristine bulk ZnO had better catalytic ability than grinded powders. One probable reason was that a large amount of structural defects, especially the bulk defects produced by ball milling lead to the decrease of the photocatalytic activity.

In the end, we can conclude that ZnO is an efficient photocatalysts to remove the organic pollutant from waste water. Photocatalytic degradation method is beneficial to the natural ecological environment and has a good development prospect.

Reference

[1] Catoor, T., European legislation relating to textile dyeing In Environmental aspects of textile dyeing Christie, R. M., Ed. Woodhead Publishing Limited: Cambridge, 2007; pp 1-29.

[2] Spagni, A.; Grilli, S.; Casu, S.; Mattioli, D., International Biodetorioration and Biodegradation 2010, 64, 676-681.

[3] Koprivanac, N.; Kusic, H., Hazardous Organic Pollutants in Colored Wastewaters. Nova Science Publishers: New York, 2009.

[4] Mahmoodi, N. M.; Arami, M., Journal of Photochemistry and Photobiology B: Biology 2009, 94, 20-24.

[5] Somensia, C. A.; L, E.; Simionattoa; L, S.; Bertoli; Jr, A. W.; Radetskib, C. M., Journal of Hazardous Materials 2010, 175, 235-240.

[6] Fujishima, Akira, and Kenichi Honda. "Electrochemical photolysis of water at a semiconductor electrode." nature 238.5358 (1972): 37.

[7] Carey, John H., John Lawrence, and Helle M. Tosine. "Photodechlorination of PCB's in the presence of titanium dioxide in aqueous suspensions." Bulletin of Environmental Contamination and Toxicology 16.6 (1976): 697-701.

[8] Katoh, Ryuzi, et al. "Efficiencies of electron injection from excited N3 dye into nanocrystalline semiconductor (ZrO2, TiO2, ZnO, Nb2O5, SnO2, In2O3) films." The Journal of Physical Chemistry B 108.15 (2004): 4818-4822.

[9] Chakrabarti, Sampa, and Binay K. Dutta. "Photocatalytic degradation of model textile dyes in wastewater using ZnO as semiconductor catalyst." Journal of hazardous materials 112.3 (2004): 269-278.

[10] Witt, Otto N. "Zur kenntniss des baues und der bildung färbender kohlenstoffverbindungen." Berichte der deutschen chemischen Gesellschaft 9.1 (1876): 522-527.

[11] Hewitt, John Theodore, and Herbert Victor Mitchell. "CXVII.—Colour and constitution of azo-compounds. Part I." Journal of the Chemical Society, Transactions 91 (1907): 1251-1266.

[12] Dilthey, W., and R. Wizinger. "Extension of Witt's color theory on coordination chemical grounds." J. prakt. Chem 118 (1928): 321.

[13] Christie, R. M., Colour Chemistry. Royal Society of Chemistry: 2001.

[14] Broadbent, A. D., Basic Principles of Textile Coloration. Society of Dyers and Colourists: West Yorkshire, England, 2001.

[15] Shore, J., Classification and general properties of colorants In Colorants and Auxiliaries Organic Chemistry and Appllication Properties

[16] Broadbent, A. D., Basic Principles of Textile Coloration. Society of Dyers and Colourists: West Yorkshire, England, 2001.

[17] Shore, J., Classification and general properties of colorants In Colorants and Auxiliaries Organic Chemistry and Appllication Properties 2ed.; Shore, J., Ed. Society of Dyers and Colourists: West Yorkshire, UK, 2002, 1, 1-44.

[18] Zuorro, Antonio, and Roberto Lavecchia. "Evaluation of UV/H2O2 advanced

oxidation process (AOP) for the degradation of diazo dye Reactive Green 19 in aqueous solution." Desalination and water treatment 52.7-9 (2014): 1571-1577.
[19] Li, Jiangtian, and Nianqiang Wu. "Semiconductor-based photocatalysts and photoelectrochemical cells for solar fuel generation: a review." Catalysis Science & Technology 5.3 (2015): 1360-1384.
[20] K. Pirkanniemi and M. Sillanpää, "Heterogeneous water phase catalysis as an environmental application: a review.," Chemosphere, vol. 48, no. 10, pp. 1047–60, Sep. 2002.
[21] Y. Matatov-Meytal and V. Barelko, "Cloth catalysts for water denitrification: II. Removal of nitrates using Pd–Cu supported on glass fibers," Applied Catalysis B: Environmental, vol. 31, pp. 233–240, 2001.
[22] Y. C. Kong, D. P. Yu, B. Zhang, W. Fang, and S. Q. Feng, "Ultraviolet-emitting ZnO nanowires synthesized by a physical vapor deposition approach," Applied Physics Letters, vol. 78, no. 4, p. 407, 2001.
[23] F. Lu, W. Cai, and Y. Zhang, "ZnO Hierarchical Micro/Nanoarchitectures: Solvothermal Synthesis and Structurally Enhanced Photocatalytic Performance," Advanced Functional Materials, vol. 18, no. 7, pp. 1047–1056, Apr. 2008.
[24] K. Pirkanniemi and M. Sillanpää, "Heterogeneous water phase catalysis as an environmental application: a review.," Chemosphere, vol. 48, no. 10, pp. 1047–60, Sep. 2002.
[25] Hoffmann, M. R.; Martin, S. T.; Choi, W.; Bahnemann, D. W. Chem. Rev. 1995, 95, 69-96.
[26] Fujishima, A.; Rao, T. N.; Tryk, D. A. J. Photochem. Photobiol. C 2000, 1, 1-21.
[27] Pardeshi, S. K.; Patil, A. B. Solar Energy, 2008, 82, 700-705.
[28] Mohsin D., Juda A. and Mashkour M.," Thermodynamic and Kinetic Study for Aromatic Rings Effect on The Photooxidation rate". International Journal of Engineering & Technology IJET-IJENS ,13 (4) (2013) 34-41
[29] Saravanana R., Shankara H., Prakasha T., Narayananb V. and Stephena A.," ZnO/ CdO composite nanorods for photocatalytic degradation of methylene blue under visible light". Materials Chemistry and Physics, 125 (2011) 277–280
[30] Lam S., Sin J., Abdullah A., Mohamed A., "Degradation of wastewaters containing organic dyes photocatalysed by zinc oxide: a review". Desalination and Water Treatment, 41 (1-3) (2012) 131-169
[31] Sobana, N., and M. Swaminathan. "The effect of operational parameters on the photocatalytic degradation of acid red 18 by ZnO." Separation and purification technology 56.1 (2007): 101-107.
[32] Xie, Juan, et al. "Simple fabrication and photocatalytic activity of ZnO particles with different morphologies." Powder Technology 207.1-3 (2011): 140-144.
[33] Danwittayakul, Supamas, Mayuree Jaisai, and Joydeep Dutta. "Efficient solar photocatalytic degradation of textile wastewater using ZnO/ZTO composites." Applied Catalysis B: Environmental 163 (2015): 1-8.
[34] Siuleiman, Shahin, et al. "Photodegradation of Orange II by ZnO and TiO2 powders and nanowire ZnO and ZnO/TiO2 thin films." Colloids and surfaces A: Physicochemical and engineering aspects 460 (2014): 408-413.

[35] Pokropivny, V. V., and V. V. Skorokhod. "Classification of nanostructures by dimensionality and concept of surface forms engineering in nanomaterial science." Materials Science and Engineering: C 27.5-8 (2007): 990-993.
[36] Ping L Yi，Hadjipanayis G C，Sorensen C M，et a1．Magnetic properties of finecobalt particles prepared by metal atom reduction．J．Appl．Phys.，1 990，67，4502．4504
[37] BMl P，Garwin L．Science at the atomic scale．Nature，1992，335，761-766
[38] Hagfeldt A，Graetzel Michael．Light-Induced Redox Reactions in Nanocrystalline Systems．1 995，95，49—68 Leggett A J，Chakravarty S，Dorsey A T，et a1．Dynamics of the dissipative two-state system Rev. Mod. Phys.，1 987，59，1—85．
[39] Wang Y Herron N．Nanometer-sized semiconductor clusters：materials synthesis，quanturn size effects，and photophysical properties. J. Phys. Chem. ，1991，95，525-532
[40] Mie, G. "Optical properties of colloidal gold solutions." Ann. Phys 25.329 (1908): 230.
[41] Link, Stephan, and Mostafa A. El-Sayed. "Shape and size dependence of radiative, non-radiative and photothermal properties of gold nanocrystals." International reviews in physical chemistry 19.3 (2000): 409-453.
[42] Link, Stephan, and Mostafa A. El-Sayed. "Shape and size dependence of radiative, non-radiative and photothermal properties of gold nanocrystals." International reviews in physical chemistry 19.3 (2000): 409-453.
[43] Nozik, Arthur J., and Rüdiger Memming. "Physical chemistry of semiconductor− liquid interfaces." The Journal of Physical Chemistry 100.31 (1996): 13061-13078.
[44] Haruta, Masatake. "Size-and support-dependency in the catalysis of gold." Catalysis today 36.1 (1997): 153-166.
[45] Mori K，Araki T，Takasaki T，el a1．A new application of photocatalysts：synthesis of nano-sized metal and alloy catalysts by a photo-assisted deposition method．Photochem．Photobi01．Sci.，2009，8(5)：652—656
[46] Weeber A W，Bakker H Amorphization by ball milling．A review．Physical B，1998，153(1—3)：93-135
[47]]Zhang D L．Processing of advanced materials using high energy mechanical milling．Progress in Materials Science，2004，49(3—4)：537-560
[48] Nath, A. K., Chongtham Jiten, and K. Chandramani Singh. "Influence of ball milling parameters on the particle size of barium titanate nanocrystalline powders." Physica B: Condensed Matter 405.1 (2010): 430-434
[49] Ksiażek, K., et al. "Investigation of the effect of intensive ball milling in a planetary ball mill on the thermal decomposition of cadmium carbonate and basic zinc carbonate." Journal of Physics: Conference Series. Vol. 79. No. 1. IOP Publishing, 2007.
[50] Rasib, Siti Zalifah Md, and Zuhailawati Hussain. "Effect of milling speed on properties of Fe-NbC composite prepared by mechanical alloying." Key Engineering Materials. Vol. 471. Trans Tech Publications Ltd, 2011.
[51] Lyu, Honghong, et al. "Ball-milled carbon nanomaterials for energy and

environmental applications." ACS Sustainable Chemistry & Engineering 5.11 (2017): 9568-9585
[52] Song, Myoung Youp, et al. "Hydrogen storage properties of a Mg–Ni–Fe mixture prepared via planetary ball milling in a H2 atmosphere." International Journal of Hydrogen Energy 35.19 (2010): 10366-10372.
[53] Anno, H., et al. "Preparation of conducting polyaniline–bismuth nanoparticle composites by planetary ball milling." Journal of electronic materials 38.7 (2009): 1443-1449.
[54] Wall, Clemens, et al ."Production of nanocrystalline lithium fluoride by planetary ball-milling." Powder technology 264 (2014): 409-417.
[55] Zhu, Kaixing, et al. "Mechanically exfoliated gC 3 N 4 thin nanosheets by ball milling as high performance photocatalysts." RSC Advances 5.69 (2015): 56239-56243
[56] Hassani, Aydin, et al. "Preparation of magnetite nanoparticles by high-energy planetary ball mill and its application for ciprofloxacin degradation through heterogeneous Fenton process." Journal of environmental management 211 (2018): 53-62
[57] Hao, Qiang, et al. "A highly efficient gC 3 N 4/SiO 2 heterojunction: the role of SiO 2 in the enhancement of visible light photocatalytic activity." Physical Chemistry Chemical Physics 18.46 (2016): 31410-31418.
[58] Wang, Yong, et al. "Facile one‐pot synthesis of nanoporous carbon nitride solids by using soft templates." ChemSusChem: Chemistry & Sustainability Energy & Materials 3.4 (2010): 435-439.]
[59] Cai, Qifeng, et al. "Template-free preparation and characterization of nanoporous g-C3N4 with enhanced visible photocatalytic activity." Journal of Alloys and Compounds 628 (2015): 372-378.
[60] Carneiro, J. O., et al. "Synthesis of iron-doped TiO 2 nanoparticles by ball-milling process: the influence of process parameters on the structural, optical, magnetic, and photocatalytic properties." Journal of Materials Science 49.21 (2014): 7476-7488.
[61] Choi, Young In, et al. "Band gap-engineered ZnO and Ag/ZnO by ball-milling method and their photocatalytic and Fenton-like photocatalytic activities." Applied Surface Science 356 (2015): 615-625.
[62] Reddy, I. Neelakanta, et al. "Effect of ball milling on optical properties and visible photocatalytic activity of Fe doped ZnO nanoparticles." Materials Science and Engineering: B 240 (2019): 33-40.
[63] https://www.fritsch-international.com/sample-preparation/milling/planetary-mills/details/product/pulverisette-7-premium-line/technical-details/
[64] Jagadish, Chennupati, and Stephen J. Pearton, eds. Zinc oxide bulk, thin films and nanostructures: processing, properties, and applications. Elsevier, 2011.
[65] ZnO 基复合材料的制备、发光及光催化性能研究. 王丽晶 2015.
[66] Zhang, Liwu, et al. "Photocorrosion suppression of ZnO nanoparticles via hybridization with graphite-like carbon and enhanced photocatalytic activity." The Journal of Physical Chemistry C 113.6 (2009): 2368-2374.

[67] Nezamzadeh -Ejhieh, Alireza, and Hamidreza Zabihi-Mobarakeh. "Heterogeneous photodecolorization of mixture of methylene blue and bromophenol blue using CuO-nano-clinoptilolite." Journal of Industrial and Engineering Chemistry 20.4 (2014): 1421-1431.
[68] Ajmal, Anila, et al. "Principles and mechanisms of photocatalytic dye degradation on TiO 2 based photocatalysts: a comparative overview." Rsc Advances 4.70 (2014): 37003-37026.
[69] Hagfeldt, Anders, and Michael Graetzel. "Light-induced redox reactions in nanocrystalline systems." Chemical reviews 95.1 (1995): 49-68.
[70] Chen, Daimei, et al. "Influence of defects on the photocatalytic activity of ZnO." The Journal of Physical Chemistry C 118.28 (2014): 15300-15307.
[71] Liu, Di, et al. "Defect-related photoluminescence and photocatalytic properties of porous ZnO nanosheets." Journal of Materials Chemistry A 2.37 (2014): 15377-15388.
[72] Zhang, Xinyu, et al. "Effect of aspect ratio and surface defects on the photocatalytic activity of ZnO nanorods." Scientific reports 4 (2014): 4596.
[73] Fang, Jiawen, et al. "Surface defects control for ZnO nanorods synthesized by quenching and their anti-recombination in photocatalysis." Applied Surface Science 332 (2015): 47-54.
[74] Bai, Xiaojuan, et al. "Performance enhancement of ZnO photocatalyst via synergic effect of surface oxygen defect and graphene hybridization." Langmuir 29.9 (2013): 3097-3105.
[75] Ashokkumar, Muthupandian, ed. Theoretical and experimental sonochemistry involving inorganic systems. Springer Science & Business Media, 2010.
[76] Takahashi, Hiroshi, and Kazuo Tsutsumi. "The Structural Change in Zinc Oxide in the Process of Mechanical Treatment." Bulletin of the Chemical Society of Japan 40.1 (1967): 7-11
[77] Thomas, D. G. "The exciton spectrum of zinc oxide." Journal of Physics and Chemistry of Solids 15.1-2 (1960): 86-96.
[78] Vidya, R., et al. "Energetics of intrinsic defects and their complexes in ZnO investigated by density functional calculations." Physical Review B 83.4 (2011): 045206.
[79] Eldrup, Morten M., P. G. Sanders, and J. R. Weertman. "Positron annihilation study of the influence of grain size and purity on the annealing behaviour of nano-crystalline copper." Materials Science Forum. Vol. 255. Trans Tech Publications Ltd, 1997.
[80] Ahmad, M., et al. "Graphene–Ag/ZnO nanocomposites as high performance photocatalysts under visible light irradiation." Journal of Alloys and Compounds 577 (2013): 717-727.
[81] Chen, Yuanlu, et al. "Synthesis of Se-doped ZnO nanoplates with enhanced photoelectrochemical and photocatalytic properties." Materials Chemistry and Physics 199 (2017): 416-423.
[82] Lonkar, Sunil P., Vishnu V. Pillai, and Saeed M. Alhassan. "Facile and scalable production of heterostructured ZnS-ZnO/Graphene nano-photocatalysts for

environmental remediation." Scientific reports 8.1 (2018): 1-14.
[83] Mizoguchi, T., et al. "Defect and electronic structure of TiSi2 thin films produced by co-sputterings.: Part II: Chemical bonding and electron energy-loss near-edge structures." Acta materialia 49.12 (2001): 2321-2328
[84] Ritterskamp, P., Kuklya, A., Wüstkamp, M. A., Kerpen, K., Weidenthaler, C., & Demuth, M. (2007). A titanium disilicide derived semiconducting catalyst for water splitting under solar radiation—reversible storage of oxygen and hydrogen. Angewandte Chemie International Edition, 46(41), 7770-7774.
[85] Liu, Jianjun, et al. "Reaction synthesis of TiSi2 and Ti5Si3 by ball-milling and shock loading and their photocatalytic activities." Journal of alloys and compounds 555 (2013): 375-380.
[86] Reed, Graham T., and Andrew P. Knights. *Silicon photonics: an introduction*. John Wiley & Sons, 2004.
[87] Kang, Zhenhui, et al. "Silicon quantum dots: a general photocatalyst for reduction, decomposition, and selective oxidation reactions." Journal of the American Chemical Society129.40 (2007): 12090-12091.
[88] Kuang, Li, Brian S. Mitchell, and Mark J. Fink. "Silicon nanoparticles synthesised through reactive high-energy ball milling: enhancement of optical properties from the removal of iron impurities." Journal of Experimental Nanoscience 10.16 (2015): 1214-1222.
[89] Pan, Hualong, et al. "Carbon nanotubols from mechanochemical reaction." Nano letters 3.1 (2003): 29-32.
[90] Wang, Zhengshang, et al. "Improving the adsorption ability of graphene sheets to uranium through chemical oxidation, electrolysis and ball-milling." Journal of Radioanalytical and Nuclear Chemistry 308.3 (2016): 1095-1102.
[91] Dash, Pranita, et al. "Preparation of graphene oxide by dry planetary ball milling process from natural graphite." RSC advances 6.15 (2016): 12657-12668.
[92] Munkhbayar, B., et al. "Influence of dry and wet ball milling on dispersion characteristics of the multi-walled carbon nanotubes in aqueous solution with and without surfactant." Powder technology 234 (2013): 132-140.
[93] Lyu, Honghong, et al. "Ball-milled carbon nanomaterials for energy and environmental applications." ACS Sustainable Chemistry & Engineering 5.11 (2017): 9568-9585
[94] Fu, Chenxi, et al. "Large scale fabrication of graphene for oil and organic solvent absorption." Progress in Natural Science: Materials International 26.3 (2016): 319-323.
[95] He, Guangyu, et al. "One-step ball-milling preparation of highly photocatalytic active CoFe2O4–reduced graphene oxide heterojunctions for organic dye removal." Industrial & Engineering Chemistry Research 54.11 (2015): 2862-2867.
[96] Santos, Diogo FM, et al. "Catalytic wet oxidation of organic compounds over N-doped carbon nanotubes in batch and continuous operation." Applied Catalysis B: Environmental 199 (2016): 361-371.